Drainage network evolution and patterns of sedimentation in an experimental wedge

Marc Viaplana-Muzas, Julien Babault, Stéphane Dominguez, Jean van den Driessche, Xavier Legrand

Drainage network evolution and patterns of sedimentation in an experimental wedge

Marc Viaplana-Muzas[a], Julien Babault[a] , Stéphane Dominguez[b] , Jean Van Den Driessche[c], Xavier Legrand[d]

[a] Departament de Geologia, Universitat Autònoma de Barcelona,08193 Bellaterra (Barcelona), Spain.

marc.via.mu@gmail.com, julien.babault@uab.es

[b] Géosciences Montpellier, Université Montpellier II, F-34095, France.

dominguez@gm.univ-montp2.fr

[c] Géosciences Rennes, Université de Rennes 1, Campus de Beaulieu, Rennes, France.

jean.van-den-driessche@univ-rennes1.fr

[d] Petronas CariGali, Twin Tower KLCC, 50088, Kuala Lumpur, Malaysia.

legrand.xavier@petronas.com.my

Abstract

In fold and thrust belts drainage organization and patterns of sedimentation depend conceptually on the ability or not for preexisting reaches to incise uplifting thrust sheets. In this study we investigate experimentally the dynamics of drainage network in a wedge submitted to shortening and erosion. It allows us to reproduce and to monitor the interactions between tectonics, erosion and sedimentation during the development of up to five successive thrust sheets. In the experiments channels adjust to uplift rate by both increasing their slope and narrowing their channels as it is observed in nature. The series of experiments shows that the proportion of persistent preexisting transverse channels increases with the ratio of rainfall over shortening rates. The experiments confirm the view that the competition between discharge and tectonic uplift controls along-strike variations in sediment flux in sedimentary basins by controlling the drainage organization. If the transverse channels draining a wedge are not diverted, a line-source dispersal system develops in front of the active structure. If channels are diverted in the backlimb of the frontal structure it results in point-sourced depositional systems separated by areas fed only by small channels developing in the front of the wedge. Fans accumulated in front of the active structures reveal two stages of sedimentation, one of progradation, while the frontal structure is active and a second one of valley backfilling and thrust sealing during internal deformation of the wedge.The experiments also suggest that spatial variations in rock uplift rate along a thrust front may be evidenced by minimum-discharge variations of persistent transverse channels.

Keywords:experimental modeling, accretionary wedge, drainage network organization, river diversion, sedimentation patterns, source-to-sink.

1 Introduction

The drainage network at the Earth's surface exerts a first order control on the relief dynamics and the erosion of mountain belts. Beyond its role in shaping the topography,the drainage network is a main controlling factor of the coupling between surface processes and deep crustal deformation, as well as of the relations between tectonics and climate variations, and the sedimentary record in basins. During mountain building, the drainage network development involves river diversions and captures at different scales(e.g. Babault et al., 2012; Castelltort et al., 2012; Giletycz et al., 2015)resulting in rapid changes in sediment routing and spatial distribution of erosion. Indeed, in response to folding or thrusting, transverse rivers are commonly diverted into longitudinal reaches, parallel to the structures, that gather into greater rivers, which maintain gorges through growing structures (e.g. Burbank et al., 1999; Burbank and Vergés, 1994; Jackson et al., 1996; Jolley et al., 1990; Oberlander, 1985; Talling et al., 1995). By controlling the spacing between outlets, drainage diversion may eventually control the loci of sediment supply and the stratigraphic architecture in foreland-basins (Gupta, 1997; Horton and DeCelles, 2001; Tucker and Slingerland, 1996). Conceptually, the ability or not for preexisting reaches to incise uplifting structures controls the number of diversions, and by extension drainage organization, a view confirmed by numerical models (Champel et al., 2002; Humphrey and Konrad, 2000; Koons, 1994; Koons, 1995; Sobel et al., 2003; Tomkin and Braun, 1999; van der Beek et al., 2002). In particular, numerical models, where deformation is reduced to uplift and advection over a thrust, show that the proportion of persistent preexisting transverse channels scales with the ratio of precipitation over shortening rate (Champel et al., 2002; Tomkin and Braun, 1999). Alternatively, it has been proposed that aggradation in the backlimb of emergent thrusts also helps transverse rivers to balance uplift rates allowing them to maintain their course instead of being diverted (Humphrey and Konrad, 2000), or that axial slopes, controlled by the dip of the décollement layer where the thrusts are rooted, may divert preexisting transverse channels before they reach the uplifts (Champel et al., 2002; van der Beek et al., 2002).

In this study we investigate experimentally how the interaction between drainage network and deformation controls along-strike variations in sediment flux in wedges submitted to shortening and erosion. We first investigate the similarities of behavior (geometries and kinematics) between experimental and natural channels evolving under uplifting conditions. We examine the differences in both the drainage organization and along-strike variations in sediment accumulations as a function of the ratio of rainfall rate over shortening rate. We determine the factors that control (1) the capacity for channels to incise uplifting structures and (2) the patterns of sedimentation that resulted from the drainage organization.

2 Method

2.1 Setup

The experimental set-up used in this study is adaptedfrom the setup used by Graveleau and Dominguez, (2008) and Graveleau et al., (2011). The deformation device dimensions are 80 x 150 cm and are constituted by a basal film pulled beneath a static buttress. The film is overlaid by the analogue material that models the upper part of the crust. Shortening induces material deformation and generates an accretionary wedge composed of imbricated thrusts. The rainfall system is composed by sprinklers that deliver water micro-droplets over the model. Sprinklers deliver water micro-droplets in sequences of 10 seconds with rain and 3 seconds without rain in order to improve channel incision processes.During the 3 seconds without rain, slope erosion processes are mostly inhibited whereas in the river network, water, collected by the channel catchments during the 10 seconds rain phase, continues to flow for a while (a few seconds up to tens of seconds depending on the length of the considered channel). During the dry time period, channel incision is then enhanced generating a more incised topography and favoring fluvial and alluvial terrace formation. This protocol was implemented to limit channel widening induced by the high river flow dynamics. Droplet size is small enough (diameter $\leq$ 100 μm) to reduce rain-splash effect and potential surface craterization. Rainfall in the experiment allows water runoff to generate both diffusive erosion processes on hillslopes and incision/lateral erosion in channelsbut it does not intend to simulate real water droplets(Graveleau et al., 2015). Spatial variation of rainfall rates due to air convection induced by water supply from sprinklers have been measured to be minor (<10%on average).

The analogue material is composed of three different materials: glass microbeads, silica powder and plastic powder (PVC). To obtain experiments with thrusts spaced enough to avoid the burying of thrust backlimbs by fans, we adjust the composition of material mixtures, the thickness of the material and layering of different materials. As mentioned above, aggradation in the backlimb of an uplifting thrust helps transverse rivers to balance uplift rates.Two different analogue material mixtures were derived and deposited in two layers in the sand-box. The upper layer is the material submitted to erosion and it is made up with 46% of glass microbeads, 30% of silica powder and 24% of plastic powder (PVC) plus some graphite (<1%) necessary for photo-correlations (material IV). This mixture is slightly different to the material IV used in Graveleau et al.(2008), Graveleau et al.(2011) and Strack et al., (2011). The lower layer is made of 50% of glass microbeads and 50% of PVC. We performed several tests and we found empirically that a total thickness of 55 mm made by a basal layer of 5 mm of glass microbeads (décollement layer), overlaid by 45 mm of the analog materials plus a thin layer (5 mm) of glass microbeads within the upper mixture results in 14-cm-spaced thrust sheets (Fig. 1). The thin layer of glass microbeads within the upper mixture allows slip to occur within the material IV

resulting in foldingat the surface above the ramps, as in nature. The deformation style reproduces well an accretionary wedge pattern made of individualized in-sequence thrust faults dipping toward the buttress.The material IV submitted to erosion has enough cohesion for valleys and crests to develop but not too high for basal shear stress applied by the fluid on the riverbed to exceed the thresholds for detachment and transport.

Digital Elevation Models (DEM) are acquired by an optical measurement bench composed by high resolution cameras coupled to a laser interferometer.This device acquires digital topographies at a 3D resolution close to 0.2 mm. It requires stops in both shortening and rainfall systems during 30-45 minutes to dry the uppermost 1-2 mm of the model surface and avoid bright laser points that could affect DEM resolution. Photograph cameras allow us to document the dynamical evolution of the relief by video movies and image correlation analyses(Graveleau and Dominguez, 2008). Finally, the model is cut in serial cross-sections in order to study the 3D geometry of thrusts and syntectonic deposits.

In this work we present eight experiments run under shortening rates ranging from 4 cm/h to 100 cm/h, of which six were submitted to a precipitation rate of 9 mm/h (named A1 to A6) and the other two to a precipitation rate of 18 mm/h (named B1 and B2).

2.2 Analysis of the accretionary wedges

Most of the deformation in the experimental wedges occurs by frontal accretion due to forward propagation of the thrust sequence as observed classically in experiments (e.g. Davis et al., 1983). Two domains can be differentiated in the experimental wedges. The prowedge, located in the frontal part of the wedge, and formed by forethrusts and the retrowedge located in the rear of the wedge and formed by backthrusts. Prowedge slope is ruled by the Coulomb wedge theory (Davis et al., 1983) and depends on the internal friction of the material, the basal friction and the dip angle of the décollement level (flat in our experiments). The spacing between thrusts and the dip of the thrusts also depends on the basal friction and on the total thickness of the layer but also on the mechanical resistance (cohesion) of the layer. We measured prowedge slopes, spacing between thrusts in the external part of the prowedge, when a new thrust appears, and we measured the dip of the thrusts to check if the rheology of the bulk material was equivalent in all the experiments.

2.3 Scaling

Experimental modeling is ruled by a set of geometric, kinematic and dynamic similarity criteria that imply, respectively, proportionality of length, time and forces between nature and model(Hubbert, 1951; Paola et al., 2009). Applying these similarity criteria to the Mohr-Coulomb equation and neglecting inertial forces, leads to the expression:

$$C_o^* = \rho^* \cdot L^* \quad (1)$$

where C_o^*, ρ^* and L^* are the ratios between model and nature for cohesion, density and length, respectively. We calculated the cohesion of the erodible material using a modified Hubbert-type set-up, following the methodology described in Graveleau et al. (2011). This device measures frictional properties of water-saturated granular materials. It consists of two aluminum rings, 8 cm in internal diameter and 50 cm^2 in horizontal cross-sectional area, which contain the granular material sample. The lower ring, 3 cm deep, is fixed on a mobile plateau controlled by a stepping motor. The upper ring is fixed on a rigid pendulum that rests on a force gauge. Its internal surface is covered with a low friction material (Teflon) to reduce sidewall friction. Between both rings there is a gap of 0.1 mm filled with low viscosity grease to prevent water and material from escaping. When the lower ring moves, material inside the ring is sheared and the upper ring presses the force gauge. We performed several tests with increasing normal loads to measure normal and tangential stress couples at failure and to deduce a yield locus. Displacement and force gauge data are recorded and allow for the generation of a Mohr-Coulomb failure envelope. Best fit to the data gives a slope equal to the coefficient of internal friction (μ) and an extrapolated cohesion (C_o). Results for our mixture, material IV (matIV), for stable friction, are μ = 0.67 (ϕ_{matIV} = 35º) and cohesion of C_o = 610 Pa for stabilized water saturation of 21-22 % (Fig.2).Cohesion in natural rocks ranges between 10^7 Pa for sandstone or granite and 10^8 Pa for marble and limestone(Schellart, 2000), hence the cohesion ratio C_o* ranges between $6.1 \cdot 10^{-5}$- $6.1 \cdot 10^{-6}$. Considering the bulk density of matIV (ρ_{matIV}=1600 $kg.m^{-3}$) and natural rocks (between 2000 $kg.m^{-3}$ for sandstone and 2800 $kg.m^{-3}$ for granite), the density ratio ρ* ranges between 0.57 and 0.80. According to equation (1)L^* is $1 \cdot 10^{-5}$- $8 \cdot 10^{-6}$, that is, 1 cm in the experiments equals ~0.1 kmto~1km in nature.

2.4 Analysis of the digital topographies

2.4.1 Quantification of the stream power erosion law in the experiments

We searched for relationships between metrics of the topography in the framework of the stream power theory for understanding and quantifying the landscape evolution and the drainage evolution in response to external perturbations.We analyzed the relationship between the steepness indices (a metric based on slope-area plots), the relative uplift rates as defined in

Babault et al. (2005), the upstream velocity of propagation of knickpoints, the channel widths and the drainage areas of steady-state reaches identified within the channels that cross uplifting thrust sheets. The stream power theory assumes that fluvial erosion is a power law function of the drainage area, *A*, and the channel slope, *S*, (Howard and Kerby, 1983). Stream power erosion laws have the form:

$$\frac{dz}{dt} = U - f(Q_s) \cdot K \cdot \frac{A^m}{W} \cdot S^n \quad (2)$$

where the rate of change of elevation, *z*, with time, t, depends on the imposed uplift rate, U, and on a power law function of drainage area, *A* (as a proxy for catchment discharge), channel width, *W*, and downstream channel slope, *S*. The exponents*m* and *n*are positive, $f(Q_s)$ describes the tool and cover effects of sediment supply and it is often taken to be equal to 1. In the experiments, uplifts induce waves of incision and knickpoints that propagate upstream indicating conditions close to the detachment-limited model of incision(Cowie et al., 2008; Whipple and Tucker, 2002). We consider that there is no effect of $Q_s$on erosion efficiency in the experiments and $f(Q_s)$ equals 1. *K* is a parameter describing erosional efficiency. Channel width(*W)*, may be described as a power law function of *A* (and is often taken to scale with $\sqrt{A}$)(Montgomery and Gran, 2001; Schellart, 2000; Whittaker et al., 2007a), in which case its effect can be subsumed into exponent *m* and coefficient *K*(Attal et al., 2008; Whipple and Tucker, 1999). However, it has been shown in a few settings that in response to an incrementof the uplift rate, incision rate can be increased by the narrowing of channels in order to increase the stream power(e.g. Amos and Burbank, 2007; Finnegan et al., 2005; Whittaker and Boulton, 2012; Whittaker et al., 2007a, 2007b).

At steady-state, by definition the channel erosion rate is equal to the uplift rate of rock (*E* = *U*), and the steady-state channel gradient (S_e) can be found by solving equation (2) for slope under this condition(Howard, 1980):

$$S_e = \left(\frac{WU}{K}\right)^{\frac{1}{n}} \cdot A^{-\frac{m}{n}} \quad (3)$$

The m/n ratio is predicted to depend only on the rate of increase of water discharge and channel width with drainage area(Whipple and Tucker, 1999), with a typical value of ~½ in nature. The exponents *m* and *n* reflect the mechanics of the dominant incision process, or combination of processes(Whipple, 2004). Equation (3) has the same form of Flint's law that relates the channel slope, *S*, to drainage area, *A*, with the normalized channel steepness index, k_{sn}, and concavity, θ(we used a reference concavity equal to 0.5 in this study):

$$S = k_{sn} \cdot A^{-\theta}, \quad (4)$$

Steady-state channels adjust to increasing uplift rate by increasing their slope (normalized channel steepness index,k_{sn})(Bookhagen and Strecker, 2012; DiBiase et al., 2010; Gudmundsdottir et al., 2013; Kirby and Ouimet, 2011; Kirby and Whipple, 2012; Ouimet et al., 2009; Perron and Royden, 2013; Wobus et al., 2005) and/or by narrowing their width, which

concentrates runoff and increases the stream power(Amos and Burbank, 2007; Finnegan et al., 2005; Whittaker et al., 2007a). The stream power erosion law predicts at steady-state that the relation between the erosion/uplift rate,the normalized steepness index and channel width depends on parameter *n*:

$$U = \frac{K}{W} \cdot {k_{sn}}^{n} \quad (5)$$

If channel width scales with drainage areas then equation (5) can be rewritten as:

$$U = K \cdot {k_{sn}}^{n} \quad (6)$$

We calculated the steepness indices and we measured the channel width of the steady-state reaches to understandthe way channels adjust to uplift rates.*K* is constant inthe series of experiments run under the same rainfall rate. We estimated the parameter *n* using equation (5).

The family of stream power models also predicts equation (2) takes the form of a nonlinear kinematic wave of erosion in response to external perturbation(Rosenbloom and Anderson, 1994; Royden et al., 2000; Whipple, 2001; Whipple and Tucker, 1999) and can be rewritten as:

$$\frac{\partial z}{\partial t} = -\frac{K}{W} \cdot A^{m} \cdot S^{n-1} \left|\frac{\partial h}{\partial x}\right|, \ \frac{\partial h}{\partial x} < 0 \quad (7)$$

where

$$C = \Psi_K \cdot A^{m} \cdot S^{n-1}, \text{with} \qquad \Psi_K = \frac{K}{W} \quad (8)$$

*C*is the wave celerity which has been used to represent knickpoint retreat rate(e.g. Berlin and Anderson, 2007; Bishop et al., 2005; Crosby and Whipple, 2006; Loget and Van Den Driessche, 2009; Parker and Anderson, 1977; Tucker and Whipple, 2002; Whipple and Tucker, 2002; Whittaker et al., 2008; Whittaker and Boulton, 2012; Wobus et al., 2006a; Wobus et al., 2006b)andΨ_K embeds lithological and width effects. Field evidence shows that knickpoint migration rates scalewith drainage area(e.g. Berlin and Anderson, 2007; Bishop et al., 2005; Crosby and Whipple, 2006; Loget and Van Den Driessche, 2009; Parker and Anderson, 1977)and equation (8) reduces to:

$$C = \Psi_A \cdot A^{m} \quad (9)$$

m is shown to be equal to 0.5 and Ψ_A is a coefficient of retreat efficiency ($L^{(1-2\ h)}T^{-1}$). This relationship implies that the upstream drainage area is the predominant parameter on knickpoint migration, with regard to lithology(e.g. Berlin and Anderson, 2007; Bishop and Cowell, 1997; Bishop et al., 2005; Loget and Van Den Driessche, 2009). We first estimated the parameter *m* using equation (9), we also studied the width effect on parameter *m*using a simplified version of equation (8) relating thevariables *C*, *A* and *W*:

$$C = \Psi_{AW} \cdot \frac{A^{m}}{W} \quad (10)$$

where Ψ_{AW} is the product $K \cdot S^{n-1}$ with a dimension depending on *m*.

The width (*W*)and the distance of knickpoint propagation used to calculate *C* have been measured using the GridVisual program (P. Davy, University of Rennes 1, http://terrasse.geosciences.univ-rennes1.fr/?p=1). In all the experiments we observed that the ramp dips vary at depth, with a constant dip from the trace of the thrust up to a distance of ≤ 8-10 cm. Beyond this distance the ramp flattens before rooting to the décollement layer of glass microbeads. In order to study the controls on*W*, k_{sn} and knickpoints propagation velocities (*C*) at a given uplift rate, we restricted the study of knickpoints to the first 8-10 cm from the trace of the thrust where uplift rates can be considered spatially uniform. Mean channel widths, *W*, in uplifting thrusts sheets have been calculated from three measures spaced by ~4-5 cm and located in the hanging wall of the thrust between fan apexes and knickpoints.$k_{sn}$of each pixel in the channels located in the uplifting thrust sheets have been calculated using GridVisual and they have been averaged for comparison to uplift rates. Knickpoint location corresponds to the point where channel local slopes increase downstream. The distance over which a knickpoint has propagated has been measured between the knickpoints and the point where a thrust startsto emerge. Repeated measures indicate typical error values of 1 mm. This error has been used to derive an error of the values of the knickpoint propagation velocities (*C*).

2.4.2 Quantification of erosion and uplift

To estimate the amounts of erosion and uplift rates in the experiments we subtractedthe eroded topography from reconstructed initial topographies. The initial topographies are derived by the highest values surrounding a given pixel and measured within a rectangular-moving window. The width of the window, parallel to the transverse-channel width, is determined by the widest valleys and it has been set to 80 mm from the experiment A1. The length, parallel to the transverse channels, has been set to 1 mm to take into account the folding of the initial topography.The uplift rates we calculated are relative uplift rates as defined in Babault et al. (2005). We divided the change of elevation above the apex of the fans deposited in front of the structuresby the time spanof uplift.

2.4.3 Quantification ofthe proportion of deviations

We calculate the proportion of persistent antecedent channels,*R*, defined as the ratio between the number of transverse streams cutting through the uplifted ridge and the initial number of streams(Champel et al., 2002):

$$R = \frac{N_p}{N_{ch}} \quad (11)$$

The variable *R* varies between 0 (all rivers deflected) and 1 (all rivers cut through the growing ridge). The initial number of channels has been obtained by counting the number of incisions on the surface of a thrust sheet, when it appears. This number may beaffected by processes that

merge initial channels during the growth of a structure, as valley widenning, and by deviations not controlled by the growing frontal structure but by backthrusts in the backlimb. Fan aggradation in the backlimb also helps transverse streams to maintain their course instead of being diverted (Humphrey and Konrad, 2000). The variable *R* measured in this study strictly reflects the processes of deviation by uplift.

2.4.4 Quantification of sedimentation rates

By sprinkling tinted analogue material we added time markers on the surface of the fans at the foot of the thrust sheets. Because these color layers would alter the acquisition of digital elevation models from the surface of the experiments, they were sprinkled after the digitalization of the surface. After drying, the experiments are cut and these timelines are used to calculate the sedimentation rates from the cross-sections of the fans.

3 Results

3.1 Style of deformation

We do not observe structural differences between the models. In the series, the mean slopes of the prowedge (α) range between 8º and 11º,thrust dips (ϕ) range between 20º and 30º with a mean dip of 24±2˚ and the spacing between thrust sheets is ~ 14±2 cm (Figs. 3C, 3D and 3E). These results indicate that the rheology of the material (internal friction and basal friction) is almost constant in all the models and that the pattern of deformationin the series is not influenced by the two orders of magnitude of shortening rates we applied. Experiment results also reveal that erosion has no effect on the pattern of deformation under the rates of shortening and precipitation we applied.

When a new thrust appears, it is accompanied by a small amplitude fold located above the ramp (Fig. 4A). The maximum structural offset on the thrusts is ~10 cm, most of it being completed in the initial stage of activity of a structure in the external part of the wedge. Once a new structure appears the older ones remain only weakly active. Since thrust dips are almost constant in the series of models, uplift rate is ruled by shortening rate. The faster the shortening rates, the faster the uplift rates. In most experiments we observed small thrusts rooted in the intermediate layer of glass microbeads that break the surface (offset ~1 cm). Less often we observed back thrusts with displacement <1 cm. These secondary structures have little influence on the uplift rates of the external structures.

3.2 Surface processes

In the experiments, we observe channel incision by runoff, sapping and landslide.As described in previous experiments(Graveleau et al., 2011), the high rate of precipitation (9 and 18 mm/h)we apply leads to the formation of apermanent sheet flow in the external and flat areas of the model, the thickness of which ranges between 0.5mm and 1 mm. When a new structure emerges in the external part of the wedgethe resulting slopemakes the water to converge, and channels to formleading to the onset of incision of the erodible material (Figs.4A and 4B). The small channelsrapidly grow and they attain 0.5-1 mm in depth and 2-5 mm in width (Fig.4C). Ongoing shortening and uplift trigger retreating incision on the structure and a wave of incision migrates to the backlimb of the fold-thrust, i.e.toward the inner part of the wedge (Figs. 4D, 4E and 4F).Not all of the initial channels (antecedent)succeed to cutin afold-thrust (see animation 1). We discuss in detail in the next section the controls of such behavior. Qualitatively, we observe that transverse channels with faster velocities of knickpoint retreat achieve to cross-cut the uplifting thrust sheets and we refer to them as persistent transverse channels. The number of these persistent transverse channels decreases when shortening rates increase resulting in drainage networks dominated by longitudinal reaches (Fig. 5).Lateral erosion in the channels generates terraces, which is common in such kind of experiments (Graveleau and Dominguez, 2008), and widens the valleys. The wideningof these valleys may eventually merge adjacent channels.The products of erosion are transported over a small distance that is a function of the nature of the grain. Most of the composite material (Silica Powder, PVC, Glass microbeads) accumulates at the foot of the thrust sheets, forming centimeter-scale fans by avulsion (Fig. 4D). A small fraction of the eroded products, the smaller and lighter grains of the mixture (mostly PVC), covers the flat undeformed part of the models up to15 cm to 20 cm away from the frontal structure (Fig. 4A),and another small fraction in suspension leavesthe model (<1%).

In the headwaters of the channels we observe that drainage expansion is achieved by sapping of the upper millimeter of the erodible material (Figs.6A and 6B). These results imply that erosion by groundwater flow is very limited. Landslidesmay also occur in the external limb of the compressive structures, usually in areas preserved from channelincision. A landslidecan start when the slope of the external limb becomes steeper than 20º. Normal fault scarps first appear, immediatelyfollowed by mass movement involving areas of 2×2 cm, as observed in experiment A4 (Figs.4E and 4F) and up to 20×5 cm as in experiment A6 (Figs.6C and 6D). As expected landslides aremore common at high shortening rates when the ratio between uplift and surface erosion rates reach a limit allowing the topography to attain and exceed its equilibrium slope.

The accretion of new structures in the wedge tilts the abovethrust sheetstoward the inner part (Fig. 3A), decreasing the local slopes of the topographythus inhibiting erosion. Below a threshold slope of c.a. 3˚,the cohesion of theerodiblematerial strongly decreases the erosion rate. In all the experiments we observe preserved, non-eroded surfaces. The extent of these surfaces is higher in the experiments run at ahigh shortening rate (Figs.6C and 6D).We also observe that drainage areas in the prism shrink through time, because shortening is not only accommodated by the external thrusts,but also by minor thrust reactivations within the wedge that induceunderthrusting. In experiment A6, the distance between thrusts 2 and 3 decreases from 13 cm to 10 cm after 12 cm of shortening (Figs.4B and 4F). At the scale of the whole prowedge, underthrusting results in a ~20% decrease in drainage areas.

3.3 Amounts of erosion and erosion rates

For a given precipitation rate (9 mm/h), the mean volumes of channel erosion,achieved during the activity of the external thrust sheets,show that the amount of erosion in valleys is five to twelve fold higher in the experiments running under shortening rates between 4 cm/h and 20 cm/h, compared to experiments at higher shortening rates(Fig.7A). However, volumes mobilized by landslidesarethree to four times higher at shortening rates higher than 10 cm/h.These resultsindicate that in all these experiments, surface mass balance is dominated by channel erosion and transport at shortening ratesequal to or lower than 9 cm/h (Fig.7A),and it is dominated by landslides at high shortening rates (A4 and A5).

Steady-state is never achieved at the scale of the active thrust sheets and erosion ratesare roughly one eighth of relative uplift rate (Fig.7B), far from equilibrium as evidenced from the flat surfaces preserved from erosion and from the continuing increase in elevation of the active thrust sheets. However, the channels crossing an active thrust sheet as in figure 4D do adapt to the relative uplift rates. We can see that the wave of incision propagates upstream toward the inner parts of the uplifting topography, being limited in its upstream part by a knickpoint (Fig. 8). Downstream of a knickpoint the incision rate balances the relative uplift rate, indicating that this portion of a channel is at steady-state.

3.4 Scaling erosion law with steady-state reaches

We measured the width of the steady-state channel reaches once the knickpoints have propagated in the hanging wall of the thrusts, as in figure 8C, in the series of experiments run under a precipitation rate of 9 mm/h. In thisseries, relative uplift rates vary from ~0.1 mm/minin experiment A1 up to ~2.6 mm/min inexperiment A6. Uplift rates are balanced by incision rates

in the persistent transverse channels. In all the experiments we observe that the relationship between W and A follows a power law:

$$W = W_n A^b, \quad (12)$$

where $W_n$is a reference width measurenamed width coefficient following Whittaker and Boulton (2012). Best fits are obtained for b=0.2. Channel widths narrow in responseto uplift rateas predicted by the stream power theory (Equation 5).The channel width coefficientdecreasesby a factor of three over one order of magnitude of uplift rate (Fig. 9).

Equation (3) also predicts that channels at steady-state are expected to steepen with increasing uplift rate. In particular, the stream power theory predicts that the exponent on the slope, parameter n, controls the nonlinearity between uplift rates,U, and normalized steepness indices,k_{sn} (Equation 6). Even if there is some dispersion in the data at high uplift rates, we observe a positive relation between$k_{sn}$and uplift rates, which is non-linear (Fig. 10A) in the series of experiments run under a precipitation rate of 9 mm/h:

$$U \propto {k_{sn}}^{p'} \quad (13)$$

where best fit of exponent $p'$is 2. However, we know that channels also adjust to uplift rate by narrowing. Combining the adjustment of channel steepness and width to uplift rate we obtain:

$$U \propto \frac{1}{W} \cdot {k_{sn}}^{p} \quad (14)$$

withexponent$p$=1.5±0.2 (Fig. 10B).Using both approaches we observe a non-linear relationship between channel steepness indices and uplift rates. The combination of a threshold for incision and a non-uniform distribution of discharge eventscould explain a non-linear relationship between channel steepness and erosion rate at steady-state (DiBiase and Whipple, 2011; Lague et al., 2005; Snyder et al., 2003b; Tucker, 2004). If true in the experiments, it would imply thatthe exponent p may not be equal to the parameter n in the erosion law (Equation 2). However, in the experiments rainfall rate is constantand runoff distribution events are rather uniform,implying that they should not affect erosion rates. On the other hand, downstream of the retreating knickpoints, the transverse reaches are at steady-state (Fig.8C), indicating that the threshold for incision is overcome.This suggests that the slope exponent n is higher than 1 and taking into account the width effect we infer$n$ = 1.5±0.2.

As predicted by the stream power theory (Equation 9) we obtain, in the series of experiments run under precipitation rates of 9 mm/h and 18mm/h, a power law relation between the velocity of knickpoint retreat, C, and the drainage area, A with m = 0.4. We observe that the knickpoint retreat rates are higher at higher uplift rates(Fig. 11A) as observed in nature(e.g. Loget and Van Den Driessche, 2009; Weissel and Seidl, 1998; Whittaker and Boulton, 2012) and,as predicted by the stream power theory for values of n>1 (Whipple and Tucker, 1999). This finding is consistent with the value of n recovered from the uplift rate, steepness index and width relationship.Taking into account the width effect (Equation 10), we infer$m$= 0.8±0.2, a

slightly highervalue, in the series A of experiments run under a precipitation rate of 9 mm/h(Fig. 11B).In the experimentB1run under a rainfall rate two times higher (18 mm/h), rates of knickpoint retreats are higherfor a given drainage area when compared to the experiment A1 run under 9 mm/h of rainfall. We also observe that smaller catchments managed to incise the uplifts (Fig. 11A).

3.5 Patterns of drainage network and sedimentation

During the emergence of a fold-thrust not all the preexisting-transverse channels (antecedent) (Fig.12A) succeed to cut through an uplifting thrust sheet, some antecedent channels are defeated (Fig.12B). In the model A1 at low shortening rate, most of the preexisting channels maintained their course through the emerged thrust sheet and these channels are referred to as persistent antecedent channels. In the model A2, some antecedent-transverse channels are defeated, and the discharge they lose is diverted into longitudinal channels located in the backlimb of the thrust sheets. As a consequence, the downstream part of a defeated channel that has lostits upstream area eventually drainsonly the forelimbs of the active thrusts(Fig. 12).The channels crossing an active thrust sheet adapt to the uplift rates, and if knickpoints retreat fast enough through the uplifting structure the antecedent transverse channels persist.We have shown that knickpoint retreat depends on drainage area or discharge (Fig.11A). The drainage area of a persistent channel is either initially large enough or it increases when adjacent diverted channels merge with it.

In the experiment A1, that is, at low uplift rates,75% of the antecedent channels manage to incise the uplifting thrust sheets and the 25% remaining are diverted into longitudinal reaches developed in the backlimb of the fold-thrusts (Fig. 5). At higherrates of uplift and under the same precipitation rate,<35% of the antecedent channels are persistent.As expected in the frame of the above-outlined conceptual model, the proportion of persistent antecedent channels decreases with shortening rate, i.e., with uplift rate (Fig.13A). We also observe that the proportion of persistent preexisting transverse channels, R, does not scale linearly with the ratio of precipitation over shortening rate:

$$R \propto \frac{Rainfall\ \ rate}{shortening\ \ rate}^{0.65\pm0.2} \quad (15)$$

At high R values diversions are sparse and the spacing between outlets of transverse persistent channels is low. Lower values of R mean that the spacing is higher. By controlling the spacing between the outlets of the transverse channels, the magnitude of the uplift rates also control the dispersal of the products of erosion in front of the active thrust. Low spacing between outlets leads to a line-source dispersal system where fans grow by lateral avulsion and finally coalesce in a bajada-like piedmont (Fig. 14A).Some fans are fed by larger drainage areas while most of them are small-scale fans fed by small channels that drain the external limb of the

next to last thrust sheet and the active frontal thrust sheet (Fig. 14B). At higher values of spacing between outlets, a point-sourced depositional system develops and the reduced number of fans may not merge. Large catchments feed large prograding fans that may locally bury the backlimb of the active thrust sheet (Figs. 14C and14D). We also see in figure 14 that the oldsedimentary zoneshave been incorporated into the prism as wedge-top basins (highlighted in red in Fig. 14). Although the process of wedge widening implies the incorporation of channels into larger integrated networks, we do not observe anincrease of sediment outflux, which results from a limitation of the experimental setup. The bulk of erosion in all the experiments comes mostly from the active external thrust sheet and in minor proportion from the next to last thrust sheets. Thrust sheets are back tilted when incorporated into the wedge, resulting in the decrease of channel steepness below the critical slope where erosion is strongly reduced (threshold slope of c.a. 3º).

In the experiment A1, the thickness of sediments accumulated in front of the thrust 5at t=160 min has reached~1.5 cm and in cross-section the area covered by sediments is 480 mm^2(Fig. 15A). In the experiment A4, the area of sedimentation in cross-section reached 460 mm^2 (at the same stage asFig. 15B), i.e., the volume of sediment accumulated in front of an active thrustis more or less the same whatever the shortening rate. This is explained by the fact that sediments shed by persistent channels come mainly from the erosion of the external thrust sheets during thrust activity and that the geometries of the valleys of the persistent channels are very similar in all the series of experiments. The volumes of sediment in experiments A1 and A4 have been accumulated during ~160 min and ~55 min, respectively, leading to sedimentation rates much higher in the experiment evolving under the higher shortening rate (Fig. 16).

We observe in all the experiments two sequences of aggradation. In the first one the growth of the prograding fans is evidenced by downlaps while in the second stage a thin layer of sediments seals the thrust that has become inactive (Fig. 15B). The second sequenceis almost not visible inthe cross-section of the experiment A1(Fig. 15A) because the trace of the cross-section is slightly oblique to the bottom of the valley where sediments were accumulated. Backtilting, in the backlimb of the youngestthrust sheets, triggers erosion of the distal parts of the wedge-top basins, resulting in an unconformity between the first and the second sequence. Once a basin is incorporated within the wedge deformation eventually folds both sequences and the thin second sequence may be totally eroded.

4 Discussion

4.1 Dynamics of the erosion in the experimental models and comparison to numerical models

We infer from uplift rates, incision rates and metrics of the topography that erosion in the persistent transverse channels scales nonlinearly to slope and drainage area (discharge):

$$E = K \cdot \frac{A^{0.8\pm0.2}}{W} \cdot S^{1.5\pm0.2} \quad (16)$$

The inferred exponents *m* and *n* are different to findings from other experiments undertaken at Geosciences Montpellier where*m* = *n* = 1(Graveleau et al., 2011; Strak et al., 2011). These differences likely reflect different material proportions in the mixture, since the basic materials used in the above cited experiments and in this study are the same. An exponent on the slope*n* higher than one is consistent with the high degree of knickpoint preservation. Knickpointsshould gradually become smoother with time following the stream power theoryif *n* would beless than 1 (Tucker and Whipple, 2002). The relationship between faster knickpoint celerity and large uplift rates (Fig. 11) is also explainable if *n*> 1 (Eq. 10), taking into account that the channels steepen under higher uplift rates (Fig.10). We obtain $\Psi_{AW} \propto U^{0.5\pm0.1}$ supporting *n* = 1.5 inferred from the scaling of k_{sn} with *W* and *U*.It is a higher value than inferred in studies from rates of erosion or uplift that shows that *n* vary between *n* = 1 in the Siwalik Hills, Nepal(Wobus et al., 2006a)and in Hawaii(Ferrier et al., 2013),and *n*< 1 for the same Siwalik Hills(Kirby and Whipple, 2001).Recent theoretical and field studies demonstrated a nonlinear dependence between steepness indices and erosion rates with an exponent *n* > 1 that can be explained by thresholds in the process of erosion combined to rainfall and runoff variability(DiBiase and Whipple, 2011; Finnegan, 2013; Lague, 2014). In our experiments the discharge in the persistent-transverse channels is by definition largely higher than the threshold for erosion and we do not observe temporal variations in flow velocity in these channels indicating that a threshold cannot account for the high value of *n*. The inferred high value is however consistent with some studies that inferred *n*> 1.3 in Turkey and Italy (Whittaker and Boulton, 2012) and with theoretical estimations inferring *n*to vary from 1.05 to 1.45(Attal et al., 2008). Although *m* is generally believed to be close to 0.5(e.g. Berlin and Anderson, 2007; Bishop and Cowell, 1997; Bishop et al., 2005; Loget and Van Den Driessche, 2009) we found *m* = 0.8±0.2. The experiments also show a dependence of channel width*W* to drainage area and uplift rate that implies that a simple scaling of *W* with drainage area*A* is not correct and that the experimental channels adjust to uplift rate by both increasing their slope and narrowing their width as it is observed in nature(Duvall et al., 2004; Lavé and Avouac, 2001; Snyder et al., 2003a; Turowski et al., 2009; Whittaker and Boulton, 2012; Whittaker et al., 2007a; Yanites and Tucker, 2010). The propagation of a knickpoint during the uplift of a thrust suggests that the

erosion model in the experiments is not a transport-limited model (e.g., Whipple and Tucker, 2002) except maybe in the areas of sedimentation.The model that best characterizes the areas under erosion in the experiments is a detachment-limited model or a hybrid model including transport capacity of channels(Whipple and Tucker, 2002). Our results indicate that the experimental models have geometric and kinematic similarities to what is observed in natural landscapes even if rigorous scaling is not feasibleforthese types of experiments(see discussions in Bonnet, 2009; Lague et al., 2003; Paola et al., 2009).

In the models experiencing the higher shortening rates (A5 and A6), the time for runoff-driven erosion to incise the forelimb of the uplifting thrust sheets is too short, leaving the slopes preserved from incision and submitted to generalized mass wasting. Even in dry land context, extensive non-eroded surfaces are usually not so preservedindicating that these high shortening rate experiments represent an end-member. The preservation of flatsurfaces from erosion isinherent to this kind of models, which are composed of cohesive materials that satisfy the mechanical properties for large fold-thrust to develop,in return inhibiting erosion below slopes of ~3º. However, in the models run under the slower rates of convergence, most of the erosion is achieved by runoff (Fig.6A) and the topographies dissected by channels show valleys, channels, terraces, and other features found in natural landscapes.

Until now, the influence of uplift on drainage diversion has been studied by the use of kinematic numerical models, where deformation isreduced to uplift and advection over a thrust (e.g. Champel et al., 2002; Humphrey and Konrad, 2000; Tomkin and Braun, 1999; van der Beek et al., 2002).In this study, we consider an accretionary wedge system thatallows us to reproduce and to monitor the dynamics of drainage network, erosion and sedimentation patterns,above and during the development of up to five successive thrust sheets.Onset of thrusting and spacing between thrust sheetsemerge naturally from the experiment.The deformation is controlled by the mechanical properties of the experimental material and the setup (layering and thicknesses). Except at very high rates of shortening,surface processes in the experimental models are dominated by runoff-erosion, transport (advection) and sedimentation (see also Graveleau et al., 2011 and Strak et al., 2011). In particular, this experimental setup allows investigating the effects of shortening and rainfall rates on drainage organization and sediment dispersal unlike 3D numerical studies of thrust wedges implementing 2D diffusive surface process(Ruh et al., 2013). Recently a study coupling 3D mechanical and surface process model(Collignon et al., 2014)has shown that where folds grow (thrust are not modeled) they all deviate the main channels resulting in a longitudinal-dominated network. To date no specific treatment of the controlling factors on drainage network evolution and sedimentation pattern in wedges has been done using a coupled 3D mechanical/surface process model.

4.2 Controls on spacing of persistent transverse channels

In fold-and-thrust belts drainage organization depends conceptually on the capability for preexisting reaches to incise or not uplifting thrust sheets(Jackson et al., 1996). Progradation of fans in wedge top-like basins potentially makes aggradation in the backlimb of emergent thrusts to balance uplift ratesallowingtransverse rivers to maintain theircourse instead of being diverted(Humphrey and Konrad, 2000). We designed our sand-box experiments in order forthe spacing between thrusts to be large enough (14 cm) to avoid the burying of the backlimbs (Fig.4). When a fold-thrust emerges, it propagates laterally and an axial slope parallel to the structure and perpendicular to the regional slope may be created in the backlimb. Like frontal uplift, this axial slope has, if large enough, the potential to divert preexisting transverse channels. Axial slopes are controlled by the ratio of the lateral to frontal propagation rate and by the dip of the décollement layer where the thrusts are rooted(Champel et al., 2002; van der Beek et al., 2002). In our experiments the basal décollement is flat, and when lateral growth occurs, the lateral propagation rates are 10 to 100 times higher than the convergence rates, both elements preventing the development of channel diversion by the growthof axial slopes (seefigure4B). The setup we used allows studying the influence of the rate of uplifting thrust sheet alone on channel diversion. The series of experiments shows that the proportion of persistent preexisting transverse channels, R, does not scale linearly with the ratio of precipitation over shortening rate (Fig. 13B). It has been shown numerically that thisratio scales linearly with the ratio of precipitation over shortening rateif the law of erosion is linearly proportional to the drainage area and to the slope (Champel et al., 2002; Tomkin and Braun, 1999; van der Beek et al., 2002). The scaling ofthe erosion law suggests erosionis not linearly dependent on drainage area and slope, which seems to be confirmed by the non-linear behavior of the number of diversions in response to uplift.We observe that the minimum drainage area of the persistent transverse channels increases with the rate of shortening and that it decreases under wetter conditions (Fig.11A). It means that the minimum discharge needed to overcome a new uplifting thrust sheet increases with uplift rate. Figure 17 shows that the minimum discharge increases slightly exponentially with uplift rate. Theoretically, at steady-state, discharge is proportional to uplift rate raised to the power of $1/m$. Our data follow this relation using m=0.8 ($1/m$=1.25). This relation ultimately controls the spacing of persistent transverse channels.

As mentioned above, it is generallyaccepted that the spacing of persistent antecedent rivers depends on the competition between stream power and uplift(Gupta, 1997; Jackson et al., 1996; Tomkin and Braun, 1999), although aggradation in the backlimb and the décollement dip of a thrust may complicate this simple relation(Champel et al., 2002; Humphrey and Konrad, 2000;

van der Beek et al., 2002).At the scale of an orogen, lithology does not appear to control the diversion of rivers(Gupta, 1997). Consequently, if lateral variations in drainage deflection are neither controlled by thrust geometry (décollement dip) nor by substantial changes in lithology,spatial variations in rock uplift rate along a thrust front may be evidenced by minimum-discharge variations of persistent transverse channels.

4.3 Controls on sediment dispersal

The drainage organization is an additional control on sedimentary flux to sedimentary basins. If the transverse channels draining the wedge are not diverted, a line-source dispersal system develops in front of the active structure. The merger of drainage basins results in point-sourced depositional systems separated by areas fed only by small channels developing in the external limb of the active thrust sheet. We reproduce similar sediment patternthat occurs at the Himalayan and Andean fronts(Gupta, 1997; Horton and DeCelles, 2001). The experiments confirm the view that the competition between discharge and tectonic uplift controls along-strike variations in sediment flux in sedimentary basins by controlling drainage organization(Tucker and Slingerland, 1994). The magnitude of drainage reorganization should modulate the magnitude of stratigraphic architecture variations along strike. However, we do not observe significant larger volumes of sediments in front of larger drainage basins with respect to smaller ones of the same experiments as it is observed in nature. This is an experimental limit due to the inhibition of erosion in the interior of the prism.Italso prevents the lateral expansion of drainage network in the interior of the prism, which is believed to maintain the spacing ratio of outlets (half mountain width over outlet spacing) during orogen widening(Horton and DeCelles, 2001; Hovius, 1996). In the experiments this ratio is not honored because it can only increase during widening of the prism.Once a thrust becomes inactive, it is incorporated, with its associated basin, into the prism, and minor erosion and bypass dominate. Because the spacing between thrusts is the same at different convergence rates, the time of activity of the external thrusts is lower at higher rates of shortening. This explains why the total amount of sediments delivered for different convergence rates (two orders of magnitude) does not vary although we show higher rates of sedimentation and erosion under higher rates of shortening (Fig. 16).

4.4 Prism widening

In all modelsthe spatial extent of the wedge-top basins, as well as the distance between the traces of the thrusts, both shrink through time indicating that the internal structural units are slightly underthrusted with ongoing shortening.As in previous studies we observe that the

growth of a prism fluctuates between periods of frontal accretion and internal thickening(e.g. Gutscher et al., 1996; Hoth et al., 2006; Konstantinovskaia and Malavieille, 2005; Naylor and Sinclair, 2007; Naylor et al., 2005; Simpson, 2006). Detail cross-sections of fans accumulated in front of a thrust sheet not yet active reveal two stages of sedimentation, one of progradation and a second one of backfilling and sealing of the thrust (Fig. 15B). We suggest that this two-phase sedimentary infill may be used as a marker for the transition between frontal accretion and internal growth in orogenic wedges.A proposed timescale for the activity of external thrust is 0.1-5 Myr(Naylor and Sinclair, 2007).In between periods of frontal accretion, the ratio of drainage area lost during internal growth represents ~20% of a thrust sheet initial area sincethe thrust emerged. The fluctuation between periods of frontal accretion and internal thickening, as well asdrainage area shrinking,may modulate the sedimentary flux at these timescales in foreland basins.

It is interesting to note that local slopes created by folding and faulting develop since the initial stages of tectonic growth of a wedge, and that this structurally-controlled relief is incorporated within a wedge during widening. Local slopes may divert runoff in directions perpendicular to the regional slope and create longitudinal-dominated drainage networks. Therefore tectonic-related relief may influence the long-term drainage network organization not only in the external part of an orogen but also in its interior. This can occur during the inversion of a rift (Babault et al., 2012) or during widening of a wedge by forward propagation and incorporation of thrust sheets as in the experiments.

5 Conclusions

Our results suggest that the rule of erosion in the experimental models has many similarities to what is observed in natural landscape. We infer from uplift rates, incision rates and metrics of the topography that erosion scales nonlinearly to slope and drainage area. We found for the exponents on the slope (n) and on the drainage (m) the respective values of 1.5±0.2 and 0.8±0.2. The experimental channels adjust to uplift rate by both increasing their slope and narrowing their channels as it is observed in nature above active faults.

Drainage pattern in fold-and-thrust belts depends on the capability for antecedent reaches to incise or not the uplifting thrust sheets. We observe that the minimum drainage area for transverse channels to incise the uplifting structure increases with the rate of shortening and decreases under wetter conditions, suggesting that discharge is the controlling factor. Indeed, a minimum discharge exists for a new uplifting thrust sheet to be overcome and it increases exponentially with uplift rate. This minimum discharge ultimately controls the spacing of persistent transverse channels. Consequently, if lateral variations in drainage deflection are neither controlled by thrust geometry (décollement dip) nor by substantial changes in lithology

as shown in previous studies, then the spatial variations in rock uplift rate along a thrust front could be evidenced by studying minimum-discharge variations of persistent transverse channels.

The experiments confirm the view that competing discharge and tectonic uplift control drainage pattern resulting in along-strike variations of sediment flux in sedimentary basins. When the transverse channels that drain a wedge are not diverted, a line-source dispersal system develops in front of the active thrust sheet. The merger of drainage basins in the backlimb of the frontal thrust sheet results in point-sourced depositional systems separated by areas fed by small channels that develop in the external limb.

Detail cross-sections of fans accumulated in front of a thrust sheet that became inactive reveal two stages of sedimentation, one of progradation and a second one of backfilling and sealing of the thrust. We suggest that this two-phase sedimentary infill may be used as a marker for the transition between frontal accretion and internal growth in orogenic wedges.

Acknowledgments

Financial support was provided to J. Babault by REPSOL, for M. Viaplana-Muzas PhD grant, and they also benefited from Spanish national projects (CGL2010-1516 and CONSOLIDER-Ingenio CSD2006-00041). We thank C. Romano from Géosciences Montpellier for technical assistance and we thank J. Malavieille for helpful discussions. Thanks to M. González, C. Díaz and E. Álvarez de Buergo for discussions on preliminary results of this work. We thank the editor Rob Govers, Kosuke Ueda and one anonymous reviewer for their constructive comments and suggestions that have contributed to the improvement of the manuscript.

References

Amos, C.B., Burbank, D.W., 2007. Channel width response to differential uplift. Journal of Geophysical Research: Earth Surface 112, F02010.

Attal, M., Tucker, G.E., Whittaker, A.C., Cowie, P.A., Roberts, G.P., 2008. Modeling fluvial incision and transient landscape evolution: Influence of dynamic channel adjustment. J. Geophys. Res.-Earth Surf. 113, 16.

Babault, J., Bonnet, S., Crave, A., Van Den Driessche, J., 2005. Influence of piedmont sedimentation on erosion dynamics of an uplifting landscape: An experimental approach. Geology 33, 301-304, doi: 310.1130/G21095.21091.

Babault, J., Van Den Driessche, J., Teixell, A., 2012. Longitudinal to transverse drainage network evolution in the High Atlas (Morocco): The role of tectonics. Tectonics 31, TC4020.

Berlin, M.M., Anderson, R.S., 2007. Modeling of knickpoint retreat on the Roan Plateau, western Colorado. Journal of Geophysical Research: Earth Surface 112, F03S06.

Bishop, P., Cowell, P., 1997. Lithological and Drainage Network Determinants of the Character of Drowned, Embayed Coastlines. The Journal of Geology 105, 685-700.

Bishop, P., Hoey, T.B., Jansen, J.D., Artza, I.L., 2005. Knickpoint recession rate and catchment area: the case of uplifted rivers in Eastern Scotland. Earth Surface Processes and Landforms 30, 767-778.
Bonnet, S., 2009. Shrinking and splitting of drainage basins in orogenic landscapes from the migration of the main drainage divide. Nature Geoscience 2, 897-897.
Bookhagen, B., Strecker, M.R., 2012. Spatiotemporal trends in erosion rates across a pronounced rainfall gradient: Examples from the southern Central Andes. Earth and Planetary Science Letters 327–328, 97-110.
Burbank, McLean, Bullen, Abdrakhmatov, Miller, 1999. Partitioning of intermontane basins by thrust-related folding, Tien Shan, Kyrgyzstan. Basin Research 11, 75-92.
Burbank, D.W., Vergés, J., 1994. Reconstruction of topography and related depositional systems during active thrusting. Journal of Geophysical Research: Solid Earth 99, 20281-20297.
Castelltort, S., Goren, L., Willett, S.D., Champagnac, J.-D., Herman, F., Braun, J., 2012. River drainage patterns in the New Zealand Alps primarily controlled by plate tectonic strain. Nature Geosci 5, 744-748.
Champel, B., van der Beek, P., Mugnier, J.-L., Leturmy, P., 2002. Growth and lateral propagation of fault-related folds in the Siwaliks of western Nepal; rates, mechanisms, and geomorphic signature. Journal of Geophysical Research 107.
Collignon, M., Kaus, B., May, D., Fernandez, N., 2014. Influences of surface processes on fold growth during 3-D detachment folding. Geochemistry, Geophysics, Geosystems 15, 3281-3303.
Cowie, P.A., Whittaker, A.C., Attal, M., Roberts, G., Tucker, G.E., Ganas, A., 2008. New constraints on sediment-flux–dependent river incision: Implications for extracting tectonic signals from river profiles. Geology 36, 535-538.
Crosby, B.T., Whipple, K.X., 2006. Knickpoint initiation and distribution within fluvial networks: 236 waterfalls in the Waipaoa River, North Island, New Zealand. Geomorphology 82, 16-38.
Davis, D., Suppe, J., Dahlen, F.A., 1983. Mechanics of fold-and-thrust belts and accretionary wedges. Journal of Geophysical Research: Solid Earth 88, 1153-1172.
DiBiase, R.A., Whipple, K.X., 2011. The influence of erosion thresholds and runoff variability on the relationships among topography, climate, and erosion rate. Journal of Geophysical Research: Earth Surface 116, F04036.
DiBiase, R.A., Whipple, K.X., Heimsath, A.M., Ouimet, W.B., 2010. Landscape form and millennial erosion rates in the San Gabriel Mountains, CA. Earth and Planetary Science Letters 289, 134-144.
Duvall, A., Kirby, E., Burbank, D., 2004. Tectonic and lithologic controls on bedrock channel profiles and processes in coastal California. Journal of Geophysical Research: Earth Surface 109, F03002.
Ferrier, K.L., Huppert, K.L., Perron, J.T., 2013. Climatic control of bedrock river incision. Nature 496, 206-209.
Finnegan, N., 2013. Interpretation and downstream correlation of bedrock river terrace treads created from propagating knickpoints. Journal of Geophysical Research: Earth Surface 118, 54-64.
Finnegan, N.J., Roe, G., Montgomery, D.R., Hallet, B., 2005. Controls on the channel width of rivers: Implications for modeling fluvial incision of bedrock. Geology 33, 229-232.
Giletycz, S., Loget, N., Chang, C.P., Mouthereau, F., 2015. Transient fluvial landscape and preservation of low-relief terrains in an emerging orogen: Example from Hengchun Peninsula, Taiwan. Geomorphology 231, 169-181.
Graveleau, F., Dominguez, S., 2008. Analogue modelling of the interaction between tectonics, erosion and sedimentation in foreland thrust belts. Comptes Rendus. Geoscience 340, 324-333.
Graveleau, F., Hurtrez, J.E., Dominguez, S., Malavieille, J., 2011. A new experimental material for modeling relief dynamics and interactions between tectonics and surface processes. Tectonophysics 513, 68-87.
Graveleau, F., Strak, V., Dominguez, S., Malavieille, J., Chatton, M., Manighetti, I., Petit, C., 2015. Experimental modelling of tectonics–erosion–sedimentation interactions in compressional, extensional, and strike–slip settings. Geomorphology.

759 Gudmundsdottir, M.H., Blisniuk, K., Ebert, Y., Levine, N.M., Rood, D.H., Wilson, A., Hilley,
760 G.E., 2013. Restraining bend tectonics in the Santa Cruz Mountains, California, imaged using
761 10Be concentrations in river sands. Geology 41, 843-846.
762 Gupta, S., 1997. Himalayan drainage patterns and the origin of fluvial megafans in the Ganges
763 foreland basin. Geology 25, 11-14.
764 Gutscher, M.-A., Kukowski, N., Malavieille, J., Lallemand, S., 1996. Cyclical behavior of thrust
765 wedges: Insights from high basal friction sandbox experiments. Geology 24, 135-138.
766 Horton, B.K., DeCelles, P.G., 2001. Modern and ancient fluvial megafans in the foreland basin
767 system of the central Andes, southern Bolivia: implications for drainage network evolution in
768 fold-thrust belts. Basin Research 13, 43-63.
769 Hoth, S., Adam, J., Kukowski, N., Oncken, O., 2006. Influence of erosion on the kinematics of
770 bivergent orogens: Results from scaled sandbox simulations. Geological Society of America
771 Special Papers 398, 201-225.
772 Hovius, N., 1996. Regular spacing of drainage outlets from linear mountain belts. Basin
773 Research 8, 29-44.
774 Howard, A.D., 1980. Thresholds in river regimes. Thresholds in geomorphology, 227-258.
775 Howard, A.D., Kerby, G., 1983. Channel changes in badlands. GSA Bull. 94, 739-752.
776 Hubbert, M.K., 1951. Mechanical basis for certain familiar geologic structures. Geological
777 Society of America Bulletin 62, 355-372.
778 Humphrey, N.F., Konrad, S.K., 2000. River incision or diversion in response to bedrock uplift.
779 Geology 28, 43-46.
780 Jackson, J., Norris, R., Youngson, J., Wojtal, S.F., 1996. The structural evolution of active fault
781 and fold systems in central Otago, New Zealand; evidence revealed by drainage patterns.
782 Journal of Structural Geology 18, 217-234.
783 Jolley, E., Turner, P., Williams, G., Hartley, A., Flint, S., 1990. Sedimentological response of an
784 alluvial system to Neogene thrust tectonics, Atacama Desert, northern Chile. Journal of the
785 Geological Society 147, 769-784.
786 Kirby, E., Ouimet, W., 2011. Tectonic geomorphology along the eastern margin of Tibet:
787 insights into the pattern and processes of active deformation adjacent to the Sichuan Basin.
788 Geological Society, London, Special Publications 353, 165-188.
789 Kirby, E., Whipple, K., 2001. Quantifying differential rock-uplift rates via stream profile
790 analysis. Geology 29, 415-418.
791 Kirby, E., Whipple, K.X., 2012. Expression of active tectonics in erosional landscapes. Journal
792 of Structural Geology 44, 54-75.
793 Konstantinovskaia, E., Malavieille, J., 2005. Erosion and exhumation in accretionary orogens:
794 Experimental and geological approaches. Geochem. Geophys. Geosyst. 6, Q02006.
795 Koons, P.O., 1994. Three-dimensional critical wedges: Tectonics and topography in oblique
796 collisional orogens. Journal of Geophysical Research: Solid Earth 99, 12301-12315.
797 Koons, P.O., 1995. Modeling the topographic evolution of collisional belts. Annual Review of
798 Earth and Planetary Sciences 23, 375-408.
799 Lague, D., 2014. The stream power river incision model: evidence, theory and beyond. Earth
800 Surface Processes and Landforms 39, 38-61.
801 Lague, D., Crave, A., Davy, P., 2003. Laboratory experiments simulating the geomorphic
802 response to tectonic uplift. Journal of geophysical research 108, 2008,
803 doi:2010.1029/2002JB001785.
804 Lague, D., Hovius, N., Davy, P., 2005. Discharge, discharge variability, and the bedrock
805 channel profile. Journal of Geophysical Research: Earth Surface 110, F04006.
806 Lavé, J., Avouac, J.P., 2001. Fluvial incision and tectonic uplift across the Himalayas of central
807 Nepal. Journal of Geophysical Research: Solid Earth 106, 26561-26591.
808 Loget, N., Van Den Driessche, J., 2009. Wave train model for knickpoint migration.
809 Geomorphology 106, 376-382.
810 Montgomery, D.R., Gran, K.B., 2001. Downstream variations in the width of bedrock channels.
811 Water Resour. Res. 37, 1841-1846.
812 Naylor, M., Sinclair, H.D., 2007. Punctuated thrust deformation in the context of doubly vergent
813 thrust wedges: Implications for the localization of uplift and exhumation. Geology 35, 559-562.

814 Naylor, M., Sinclair, H.D., Willett, S., Cowie, P.A., 2005. A discrete element model for
815 orogenesis and accretionary wedge growth. Journal of Geophysical Research: Solid Earth 110,
816 B12403.
817 Oberlander, T.M., 1985. Origin of drainage transverse to structures in orogens. Binghamton
818 Symposia in Geomorphology: International Series 15, 155-182.
819 Ouimet, W.B., Whipple, K.X., Granger, D.E., 2009. Beyond threshold hillslopes: Channel
820 adjustment to base-level fall in tectonically active mountain ranges. Geology 37, 579-582.
821 Paola, C., Straub, K., Mohrig, D., Reinhardt, L., 2009. The "unreasonable effectiveness" of
822 stratigraphic and geomorphic experiments. Earth-Science Reviews 97, 1-43.
823 Parker, G., Anderson, A.G., 1977. Basic principles of river hydraulics. Journal of the Hydraulics
824 Division 103.
825 Perron, J.T., Royden, L., 2013. An integral approach to bedrock river profile analysis. Earth
826 Surface Processes and Landforms 38, 570-576.
827 Rosenbloom, N.A., Anderson, R.S., 1994. Hillslope and channel evolution in a marine terraced
828 landscape, Santa Cruz, California. Journal of Geophysical Research: Solid Earth 99, 14013-
829 14029.
830 Royden, L., Clark, M., Whipple, K., 2000. Evolution of river elevation profiles by bedrock
831 incision: Analytical solutions for transient river profiles related to changing uplift and
832 precipitation rates. Eos Trans. AGU 81, 48.
833 Ruh, J.B., Gerya, T., Burg, J.-P., 2013. High-resolution 3D numerical modeling of thrust
834 wedges: Influence of décollement strength on transfer zones. Geochemistry, Geophysics,
835 Geosystems, n/a-n/a.
836 Schellart, W.P., 2000. Shear test results for cohesion and friction coefficients for different
837 granular materials: scaling implications for their usage in analogue modelling. Tectonophysics
838 324, 1-16.
839 Simpson, G.D.H., 2006. Modelling interactions between fold–thrust belt deformation, foreland
840 flexure and surface mass transport. Basin Research 18, 125-143.
841 Snyder, N.P., Whipple, K.X., Tucker, G.E., Merritts, D.J., 2003a. Importance of a stochastic
842 distribution of floods and erosion thresholds in the bedrock river incision problem. Journal of
843 Geophysical Research: Solid Earth 108, 2117.
844 Snyder, N.P., Whipple, K.X., Tucker, G.E., Merritts, D.J., 2003b. Channel response to tectonic
845 forcing: field analysis of stream morphology and hydrology in the Mendocino triple junction
846 region, northern California. Geomorphology 53, 97-127.
847 Sobel, E.R., Hilley, G.E., Strecker, M.R., 2003. Formation of internally drained contractional
848 basins by aridity-limited bedrock incision. Journal of Geophysical Research 108, 2344.
849 Strak, V., Dominguez, S., Petit, C., Meyer, B., Loget, N., 2011. Interaction between normal
850 fault slip and erosion on relief evolution: Insights from experimental modelling. Tectonophysics
851 513, 1-19.
852 Talling, P.J., Lawton, T.F., Burbank, D.W., Hobbs, R.S., 1995. Evolution of latest Cretaceous–
853 Eocene nonmarine deposystems in the Axhandle piggyback basin of central Utah. Geological
854 Society of America Bulletin 107, 297-315.
855 Tomkin, J.H., Braun, J., 1999. Simple models of drainage reorganisation on a tectonically active
856 ridge system. New Zealand Journal of Geology and Geophysics 42, 1-10.
857 Tucker, G.E., 2004. Drainage basin sensitivity to tectonic and climatic forcing; implications of a
858 stochastic model for the role of entrainment and erosion thresholds. Earth Surface Processes and
859 Landforms 29, 185-205.
860 Tucker, G.E., Slingerland, R., 1994. Erosional dynamics, flexural isostasy, and long-lived
861 escarpments: a numerical modeling study. Journal of Geophysical Research 99, 12,229-212,243.
862 Tucker, G.E., Slingerland, R., 1996. Predicting sediment flux from fold and thrust belts. Basin
863 Research 8, 329-349.
864 Tucker, G.E., Whipple, K.X., 2002. Topographic outcomes predicted by stream erosion models:
865 Sensitivity analysis and intermodel comparison. Journal of Geophysical Research: Solid Earth
866 107, 2179.

Turowski, J.M., Lague, D., Hovius, N., 2009. Response of bedrock channel width to tectonic forcing: Insights from a numerical model, theoretical considerations, and comparison with field data. Journal of Geophysical Research: Earth Surface 114, F03016.
van der Beek, P., Champel, B., Mugnier, J.-L., 2002. Control of detachment dip on drainage development in regions of active fault-propagation folding. Geology 30, 471-474.
Weissel, J.K., Seidl, M.A., 1998. Inland Propagation of Erosional Escarpments and River Profile Evolution Across the Southeast Australian Passive Continental Margin, Rivers Over Rock: Fluvial Processes in Bedrock Channels. American Geophysical Union, pp. 189-206.
Whipple, K.X., 2001. Fluvial Landscape Response Time: How Plausible Is Steady-State Denudation? Am J Sci 301, 313-325.
Whipple, K.X., 2004. Bedrock rivers and the geomorphology of active orogens. Annual Review of Earth and Planetary Sciences 32, 151-185.
Whipple, K.X., Tucker, G.E., 1999. Dynamics of the stream-power river incision model: Implications for height limits of mountain ranges, landscape response timescales, and research needs. Journal of Geophysical Research 104, 17,661-617,674.
Whipple, K.X., Tucker, G.E., 2002. Implications of sediment-flux-dependent river incision models for landscape evolution. Journal-of-geophysical-research 107, ETG3.1-ETG3.20.
Whittaker, A.C., Attal, M., Cowie, P.A., Tucker, G.E., Roberts, G., 2008. Decoding temporal and spatial patterns of fault uplift using transient river long profiles. Geomorphology 100, 506-526.
Whittaker, A.C., Boulton, S.J., 2012. Tectonic and climatic controls on knickpoint retreat rates and landscape response times. Journal of Geophysical Research: Earth Surface 117, F02024.
Whittaker, A.C., Cowie, P.A., Attal, M., Tucker, G.E., Roberts, G.P., 2007a. Bedrock channel adjustment to tectonic forcing: Implications for predicting river incision rates. Geology 35, 103-106.
Whittaker, A.C., Cowie, P.A., Attal, M., Tucker, G.E., Roberts, G.P., 2007b. Contrasting transient and steady-state rivers crossing active normal faults: new field observations from the Central Apennines, Italy. Basin Research 19, 529-556.
Wobus, C., Heimsath, A., Whipple, K., Hodges, K., 2005. Active out-of-sequence thrust faulting in the central Nepalese Himalaya. Nature 434, 1008-1011.
Wobus, C., Whipple, K.X., Kirby, E., Snyder, N., Johnson, J., Spyropolou, K., Crosby, B., Sheehan, D., 2006a. Tectonics from topography; procedures, promise, and pitfalls. Special Paper - Geological Society of America 398, 55-74.
Wobus, C.W., Crosby, B.T., Whipple, K.X., 2006b. Hanging valleys in fluvial systems; controls on occurrence and implications for landscape evolution. Journal of Geophysical Research 111.
Yanites, B.J., Tucker, G.E., 2010. Controls and limits on bedrock channel geometry. Journal of Geophysical Research: Earth Surface 115, F04019.

916
917
918
919

920 Figures and captions:

921

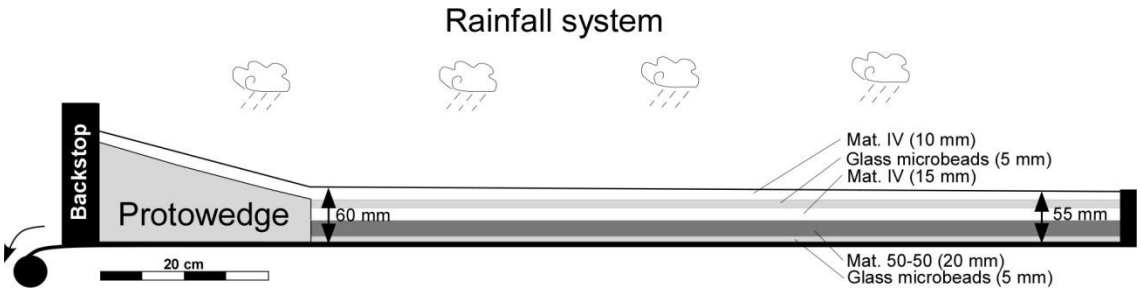

922

923 ***Figure 1.*** *Scheme of the experimental setup. We imposed a slope of 0.5º at the surface of the models in order to*
924 *enhance runoff connectivity. The initial thickness of the layered material is 60 mm close to the protowedge and 55*
925 *mm in the distal part.*

926

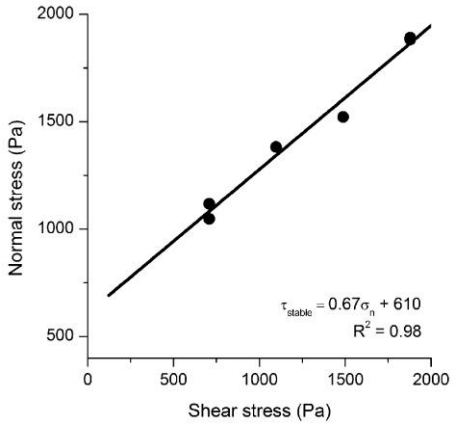

927

928 ***Figure 2.*** *Mohr–Coulomb envelope (stable friction measurements) for failure of the erodible mixture (material IV)*
929 *used in our experiments.*

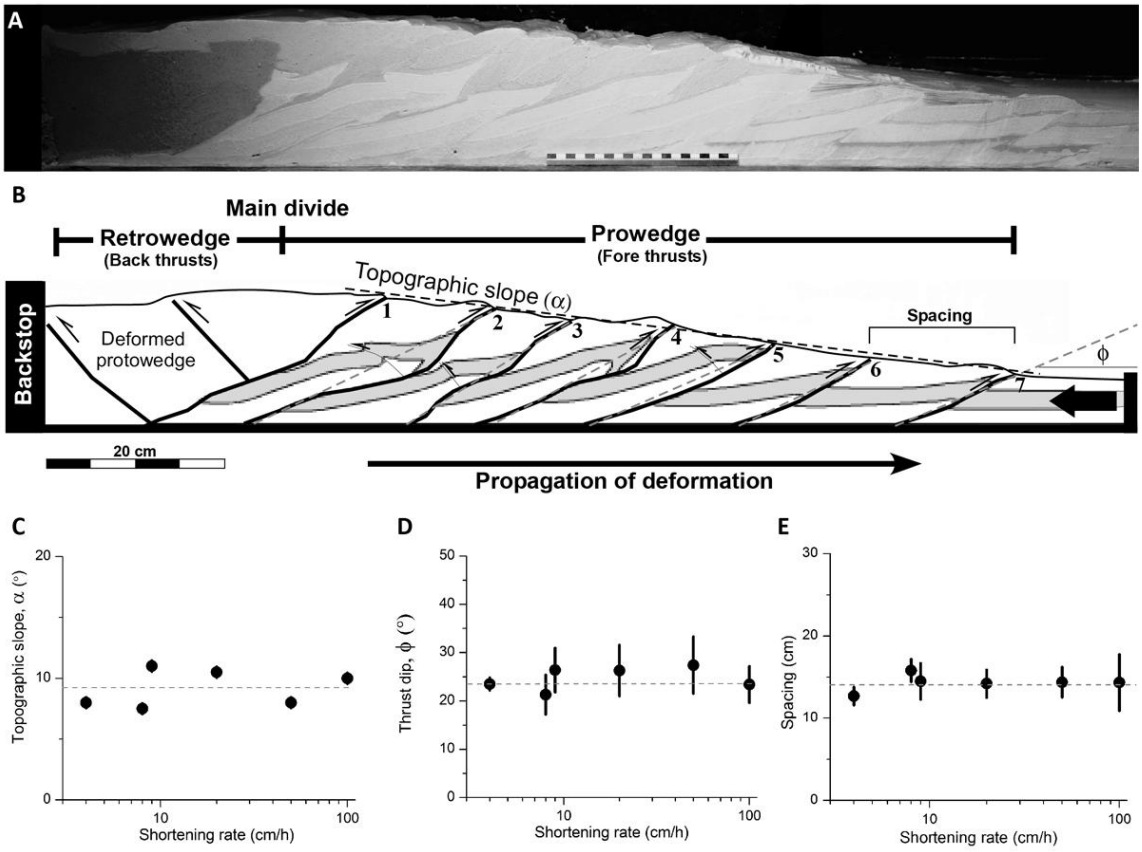

Figure 3. *(A) Cross-section of the model A4 after 1 m of shortening. (B) Interpretation showing the main thrusts. For all the experiments we calculated the topographic mean slopes (α) of the prowedges (C), the thrust dips (ϕ) measured between the root and the tip of the thrust (dashed grey lines in B) (D) and the thrust spacing measured in the external part when a new thrust emerges (E).*

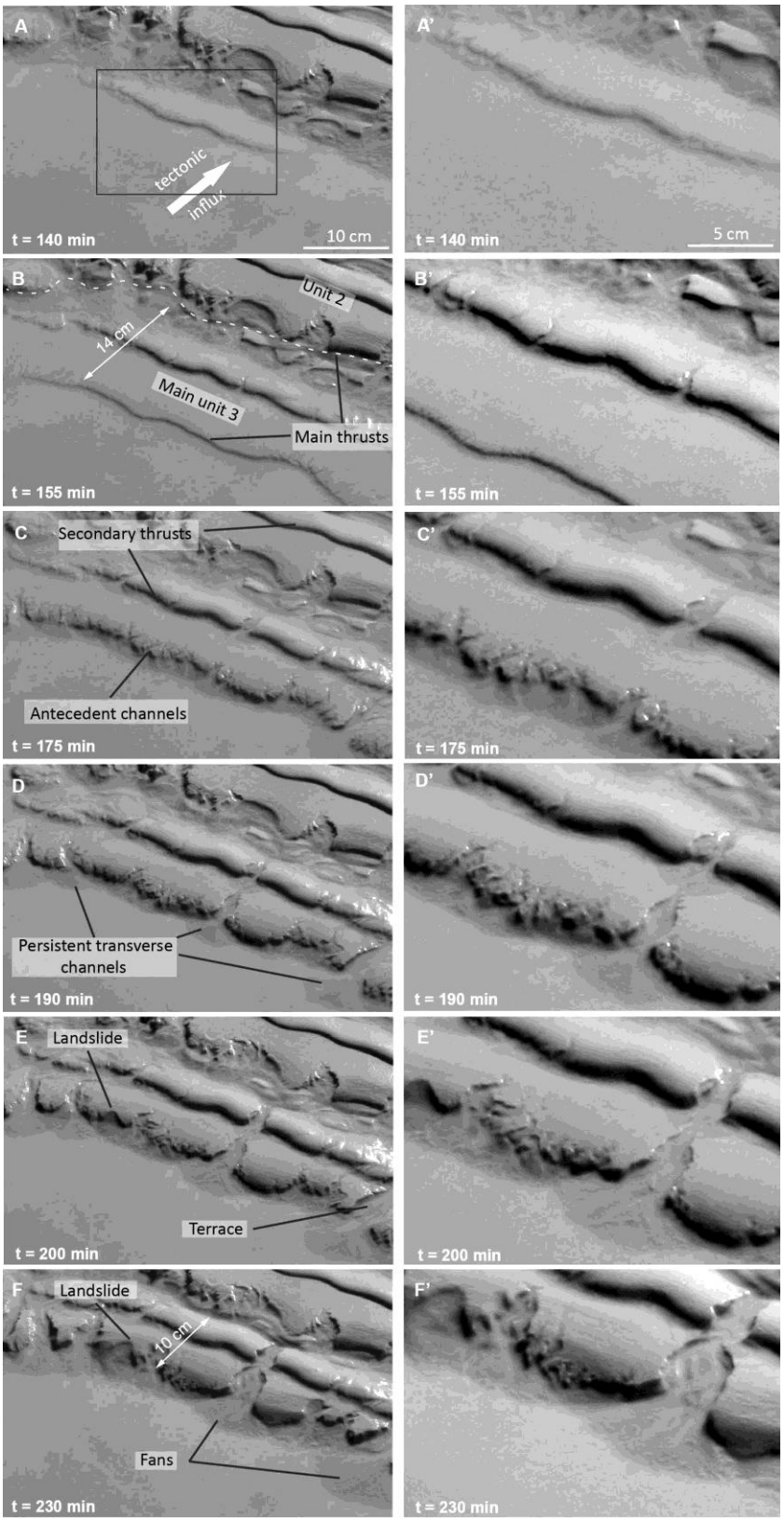

Figure 4. *Photos of the experiment, A2, from t=140 min, (A), before thrust 3 emerges, to t=230 min (F) when the third thrust sheet has totally emerged (animation 1 add in supplementary data). The amount of shortening between (A) and (F) is 12 cm.*

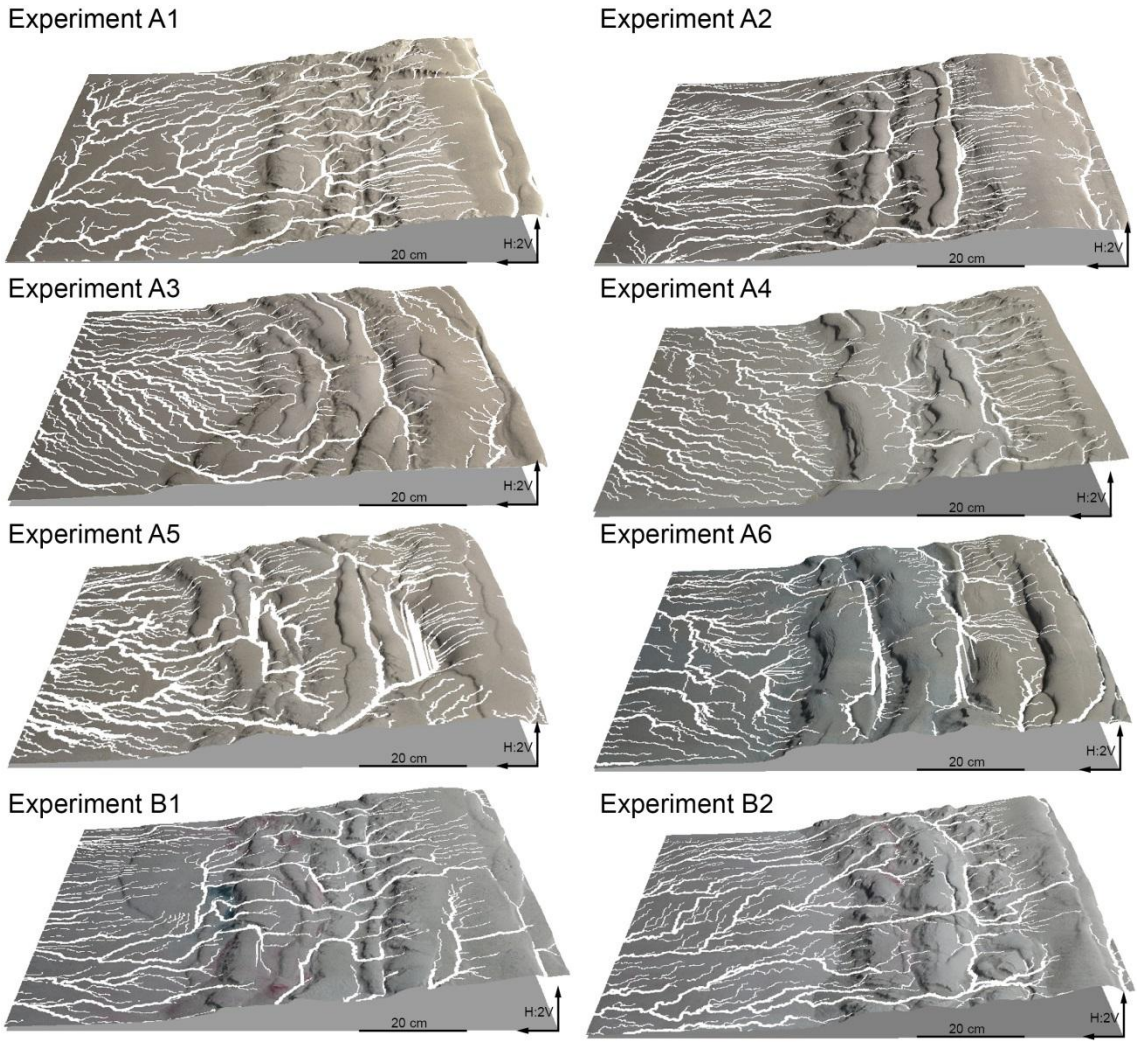

Figure 5. *3D views of all the models after the third thrust activity(the photographs are overlapped on the DEM). The drainage network is superimposed in white. The models run under 9 mm/h of rainfall rate in the A series with the shortening rate ranging between 4-100 cm/h (A1: 4 cm/h; A2: 8 cm/h; A3: 9 cm/h; A4: 20 cm/h; A5: 50 cm/h; A6: 100 cm/h). In the models run under 18 mm/h of rainfall rate, the B series, the shortening rate varied between 8 cm/h (B1) and 18 cm/h (B2).*

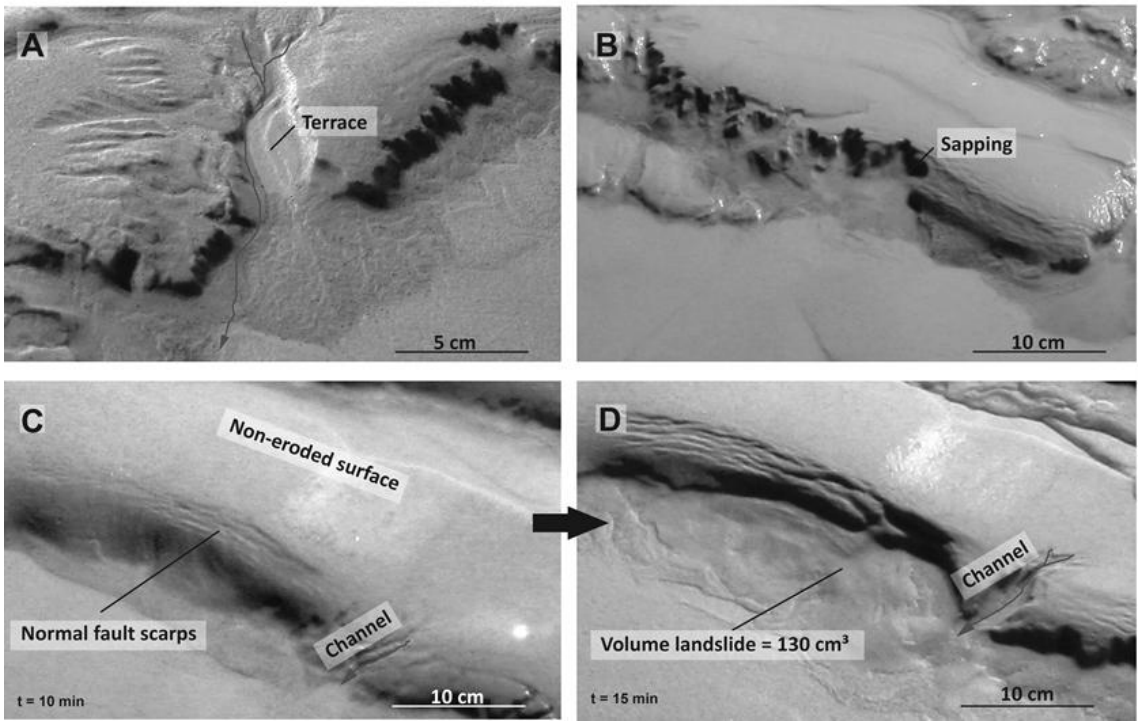

Figure 6. *Detail pictures of the principal surface processes active in experiments (A). Detail of a channel crossing the fourth thrust sheet in the experiment A4 at t= 350 min. Note the formation of a terrace in the right part of the channel and the alluvial fan located in the channel outlet. (B) Detail of sapping in the external part of the second thrust sheet of the experiment B2 at t=70 min. (C) and (D) Evolution of a landslide in the experiment A6, from t=10 min to t=15min, situated in the external part of the third thrust sheet.*

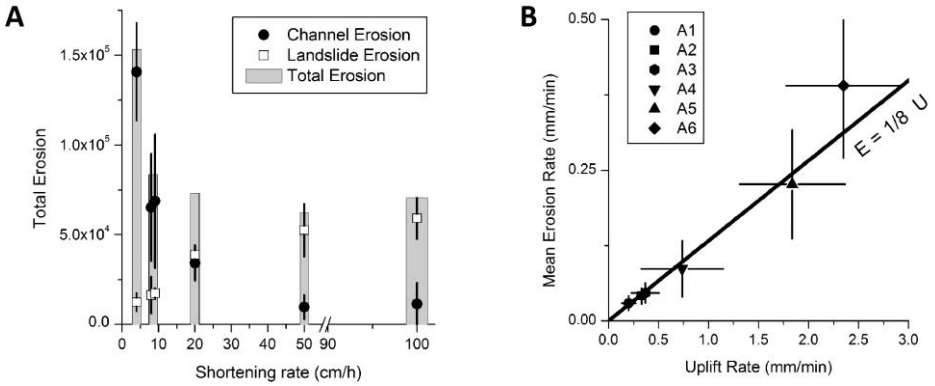

Figure 7. *(A) Mean amounts and standard deviations of erosion of the frontal thrust sheets, during their activity, calculated for experiments run under 9 mm/h of precipitation rates. (Dots) Erosion done by persistent channels and small channels developed on the forelimb of the fold-thrust. (White squares) Erosion done by landslides those develop in the forelimbs of the thrusts. (B) Mean erosion rates and standard deviations calculated from channel-driven amounts of erosion (dots in A) against uplift rate (landslide-derived erosion not included):* $E \cong \frac{1}{8} U$.

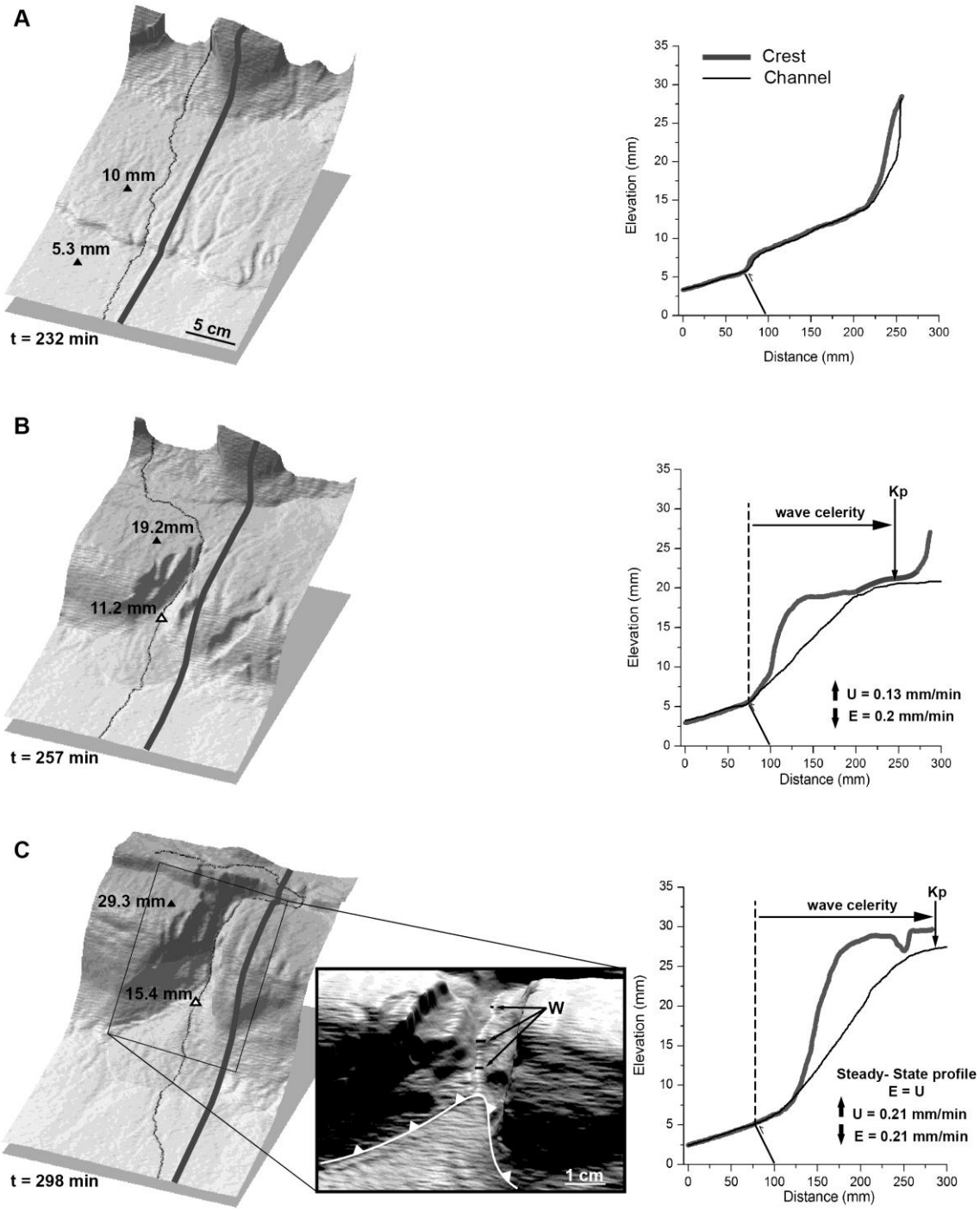

Figure 8. *(Left) 3D detail views of a persistent-channel incision during thrust activity (experiment A2). (Right) Crest and channel topographic profiles (traces superimposed on 3D views) showing the formation of a knickpoint (Kp), when the third thrust sheet starts to emerge at t=232 min (A). The knickpoint migrates upstream (B) until the fourth thrust sheet starts to emerge (C). At this moment channel erosion rate (E) balances relative uplift rate (U), 0.21 mm/min, indicating that this portion of the channel is at steady-state. The inset illustrates where the width of channels, W, has been measured along the channel. The length of the channel in this figure is 6 cm long.*

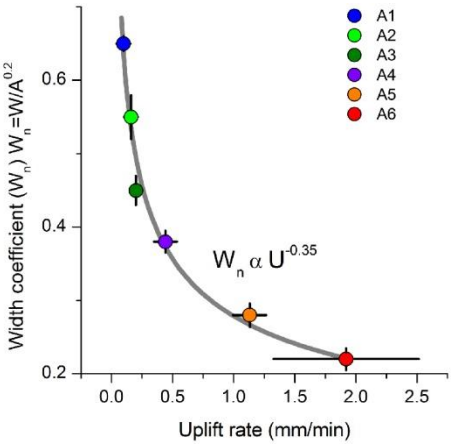

Figure 9: *Channel width coefficient, W_n (channel width normalized for drainage area), of persistent transverse channels against mean relative uplift rate (error bars are standard deviation, 1σ), in the series of experiments run under a precipitation rate of 9 mm/h. (Black line) Best fit using a non-linear regression: $W_n = 0.3 \cdot U^{-0.35}$.*

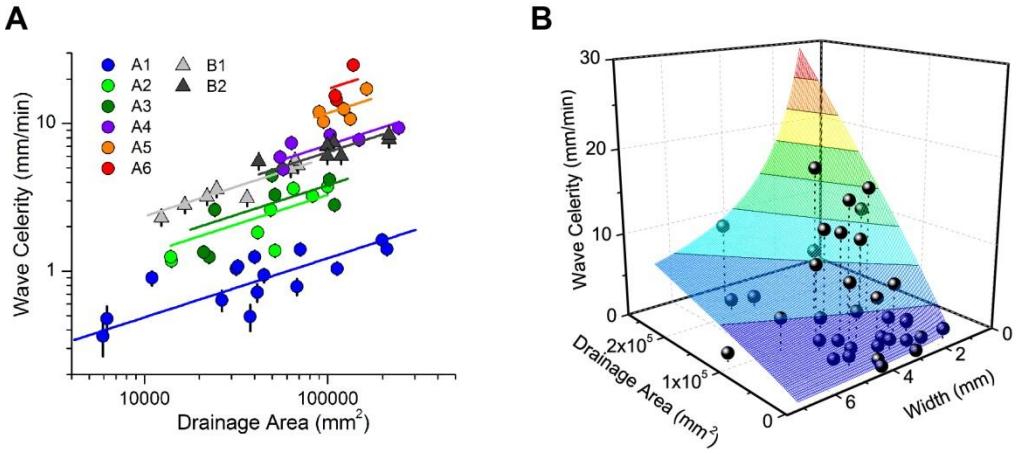

Figure 10: *(A) Normalized steepness index (k_{sn}) of the persistent antecedent channels against uplift rates, (Series A). The equation that best fits is $U=k_{sn}^2$. (B) Graphic combining the adjustment of channel steepness and width to uplift rate.*

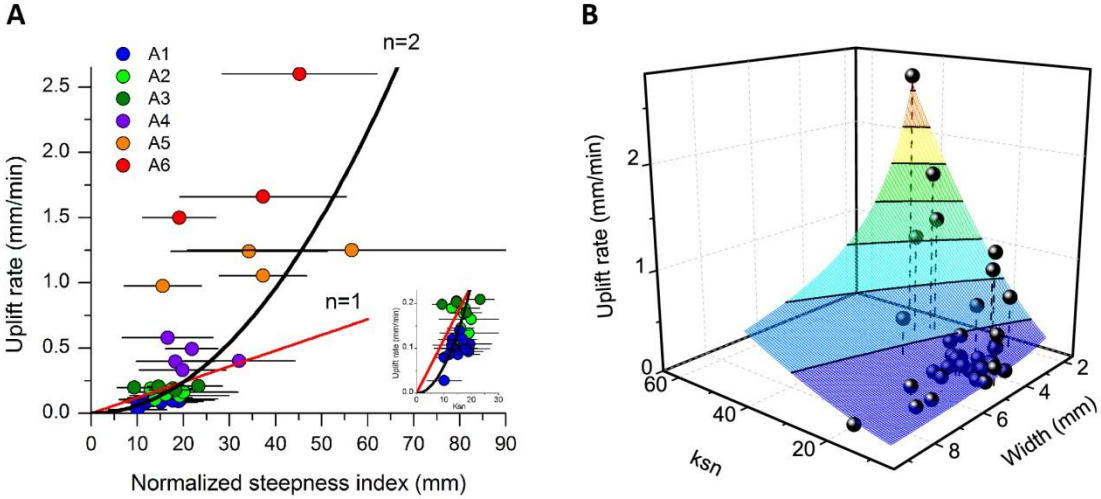

Figure 11:*(A) Knickpoint wave celerity of the antecedent persistent channels against drainage area best fit using eq. (9): $C = \Psi_A \cdot A^{0.4}$. Error bars come from the error in measuring the amount of knickpoint propagation, typically <1*

mm. (B) Knickpoint wave celerity as a function of drainage area and channels width, in the series of experiments ran under a precipitation rate of 9 mm/h, best fit using eq. (10): $C = \Psi_{AW} \frac{A^{0.8}}{W}$

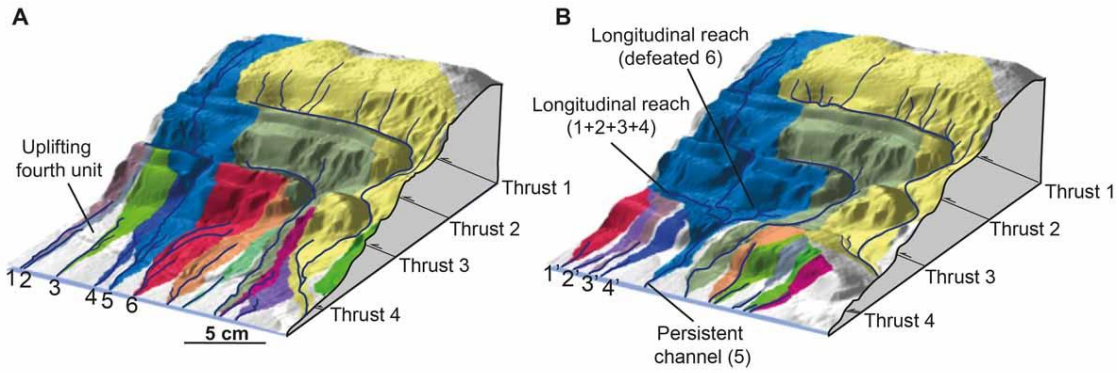

Figure 12: *Drainage areas of the catchments draining the emerging thrust sheet 4 of experiment A2 (rainfall 9 mm/h) at t=232 min (A) and at t=298 min (B). The channels 1 to 6 are pre-existing transverse channels. The antecedent channel 5 managed to cut through the uplifting thrust sheet 4 (persistent channel). Channels 1', 2', 3' and 4' are the downstream parts of the small catchments 1, 2, 3 and 4 that lost their upstream drainage area by diversion above the thrust sheet the 4 (defeated channels). Their upstream drainage areas are gathered together in the longitudinal reach of channel 5 in the backlimb of the active thrust 4.*

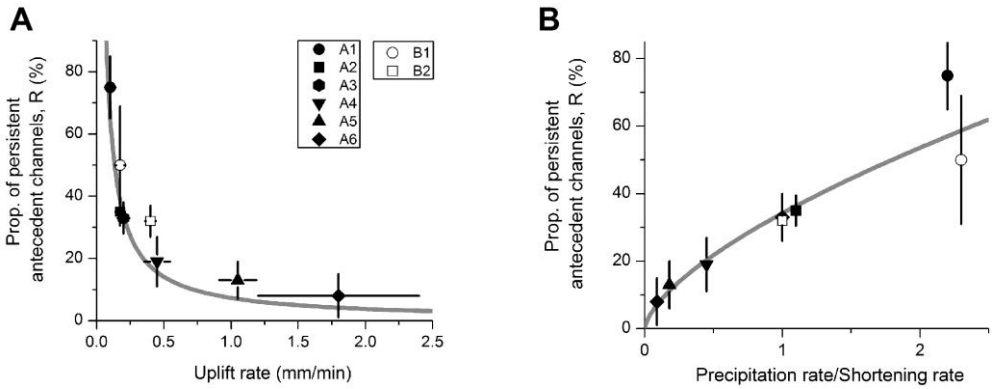

Figure 13: *(A) Proportion of persistent transverse channels against uplift rates. Note the decrease of the proportion of persistent transverse channels with the increase of the uplift rate in both series of experiments run under different rainfall rates. We obtained a good fit (R^2=98 %) using a power law regression $R=7.3 \cdot U^{-0.95}$. (B) Proportion of persistent antecedent channels against precipitation over shortening rate (labels are the same as in (A)). We obtained a good fit (R^2=98 %) using a power law regression $R=35 \cdot (Prec./Short.)^{0.65}$.*

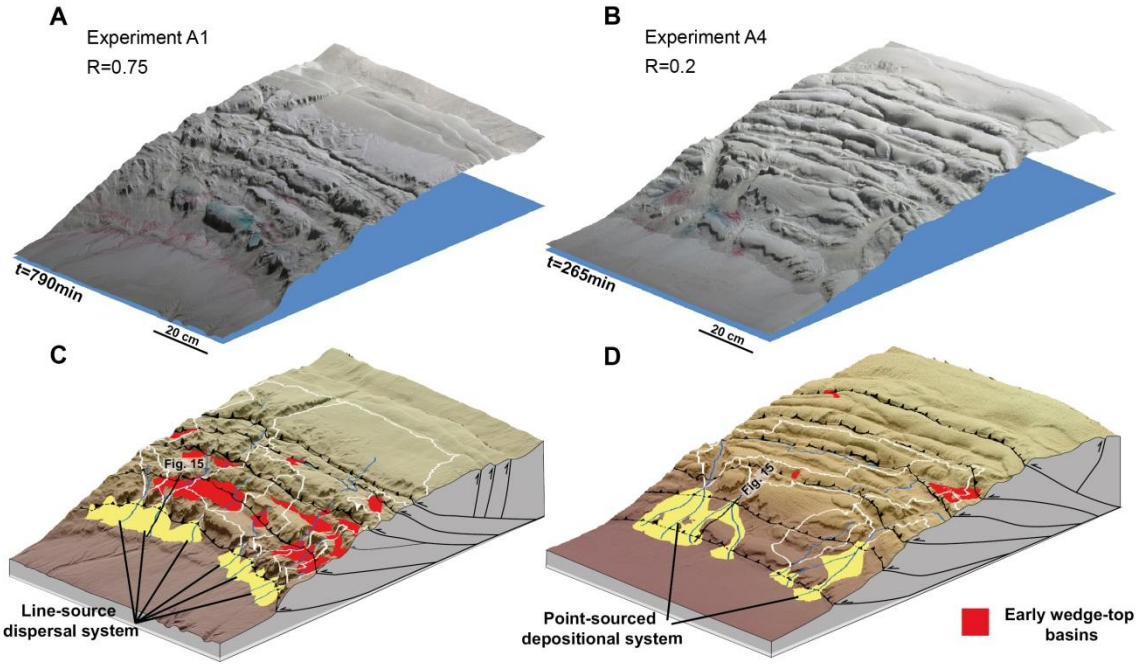

Figure 14: *Patterns of sedimentation in two experiments run under low (A) and high (B) shortening rates (rainfall is 9 mm/h). (C) Experiment A1, the high proportion of persistent transverse channels (R=75%) results in a line-source dispersal system. (D) Experiment A4, the low proportion of persistent transverse channels (R=20%) results in 2 large point-sourced depositional systems plus some small fan systems.*

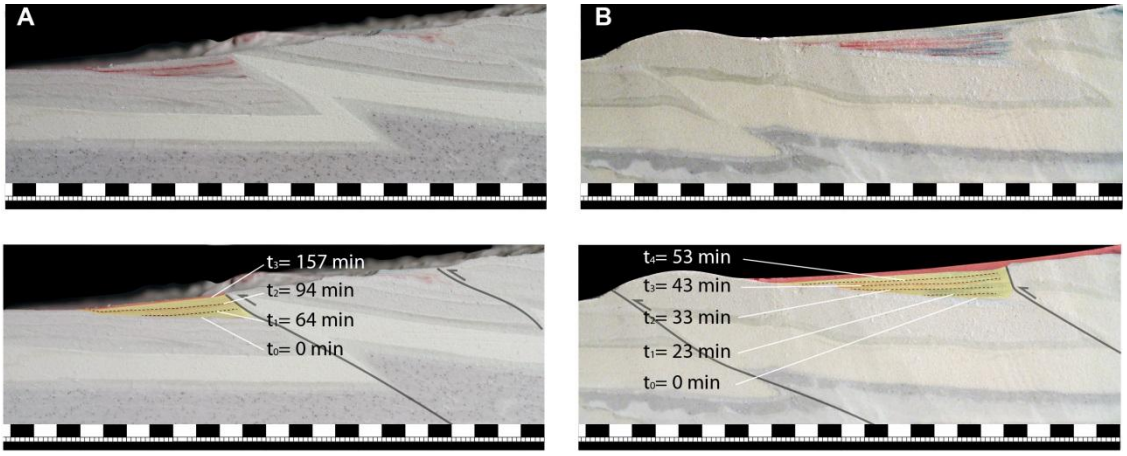

Figure 15: *(A) Detail cross-section of the sedimentation zone in front of thrust 4 in the model A1. (B) Detail cross section of the sedimentation zone in front of thrust 5 in the model A4. Photos are interpreted below and the traces of the cross sections are located in figure 14. The areas of the sedimentation zones in yellow accumulated during thrust activity and the deposits in red accumulated after thrust activity. Note that the second sequence of sediments (in red) seals the inverse faults.*

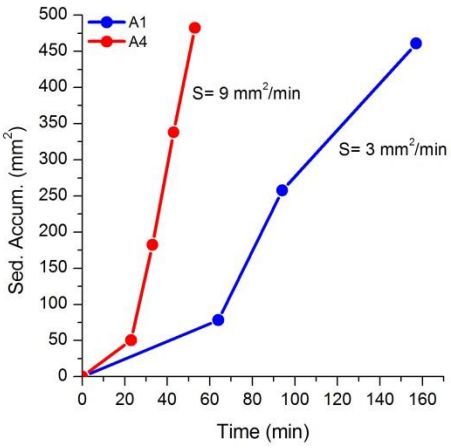

Figure 16: *Mean rates of aggradation (S) calculated from the area of sedimentation measured in the cross-sections presented in figure 15.*

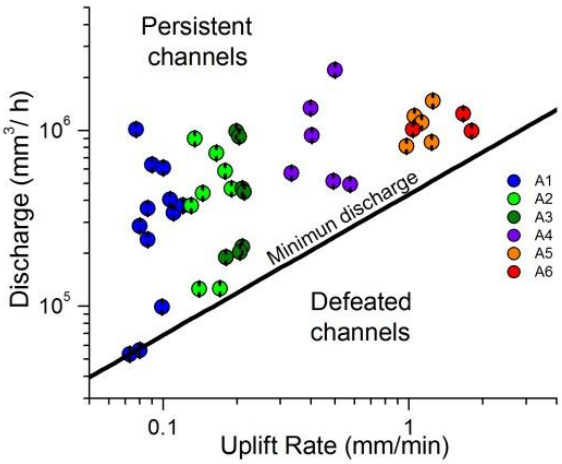

Figure 17: *Discharge of persistent transverse channels against uplift rate. Note that the minimum discharge needed to overcome a new uplifting thrust sheet increases with uplift rate. This minimum discharge increases slightly exponentially with uplift rate:* $Q_w \alpha\ U^{1/m}$ *with m=0.8.*

Figure

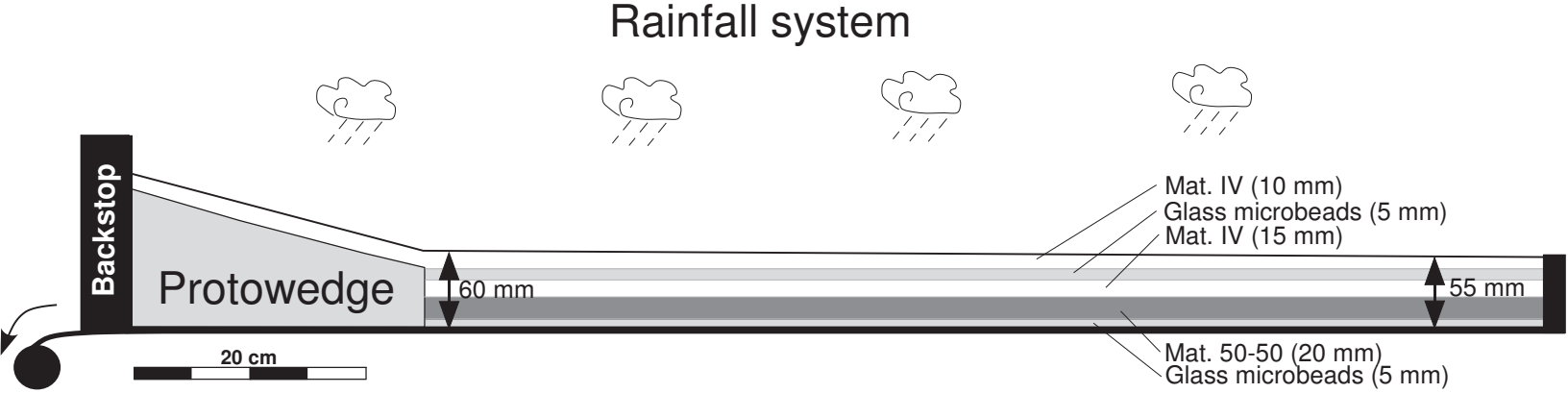
Rainfall system
Backstop
Protowedge
60 mm
Mat. IV (10 mm)
Glass microbeads (5 mm)
Mat. IV (15 mm)
55 mm
Mat. 50-50 (20 mm)
Glass microbeads (5 mm)
20 cm

Figure

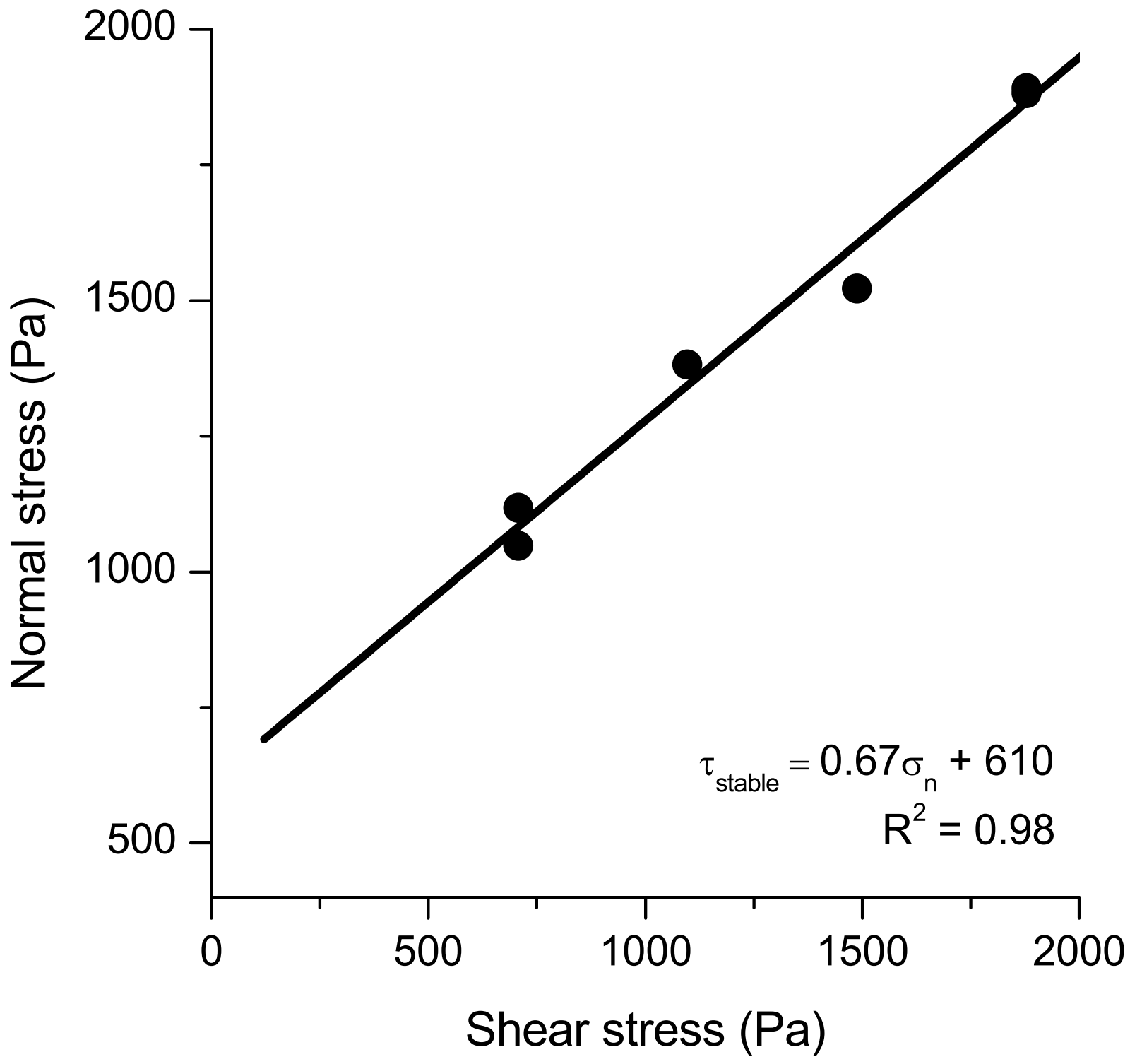
2000
1500
1000
500
Normal stress (Pa)
0
500
1000
1500
2000
Shear stress (Pa)
$\tau_{stable} = 0.67\sigma_n + 610$
$R^2 = 0.98$

Figure

Click here to download high resolution image

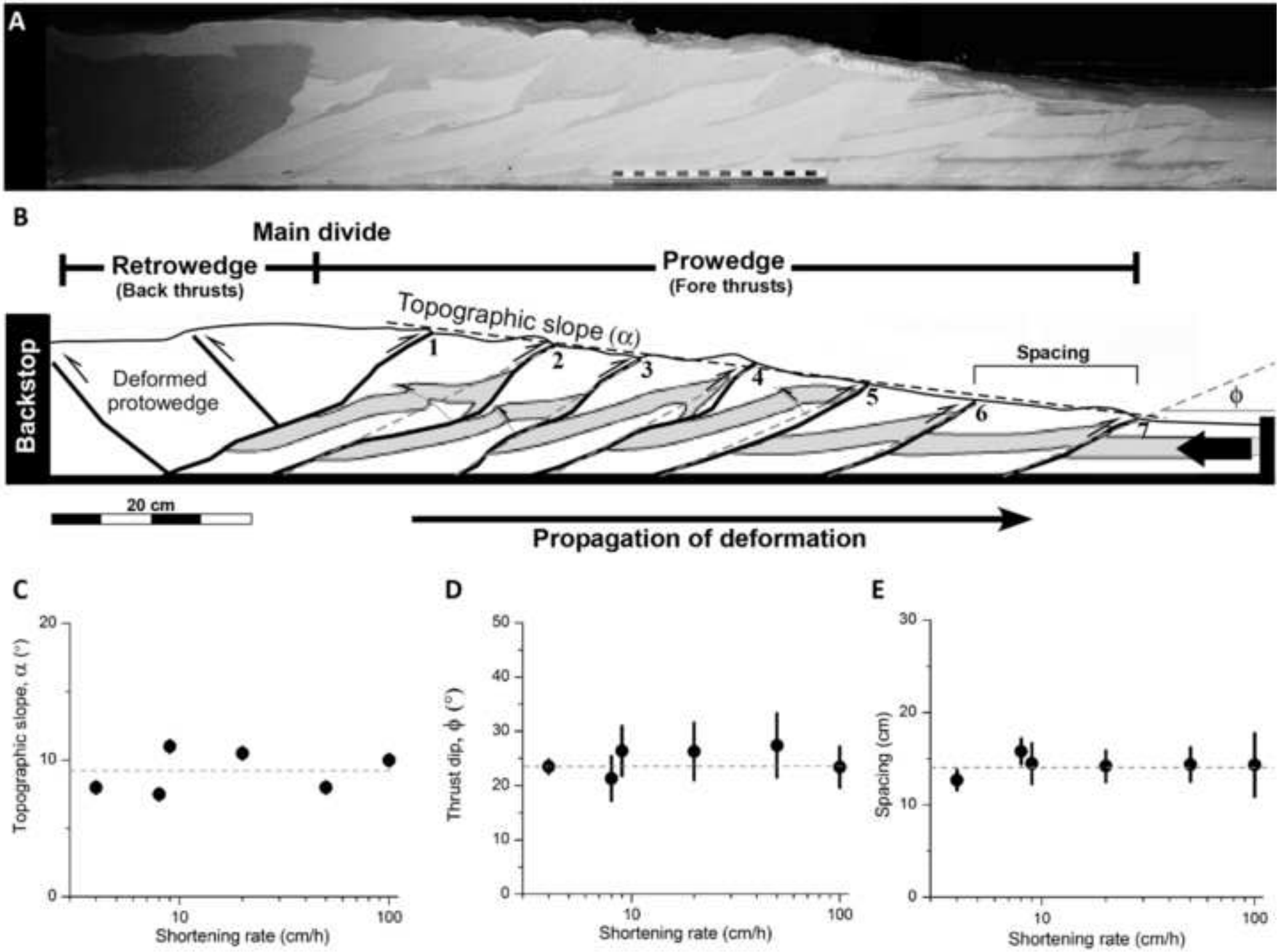

Figure

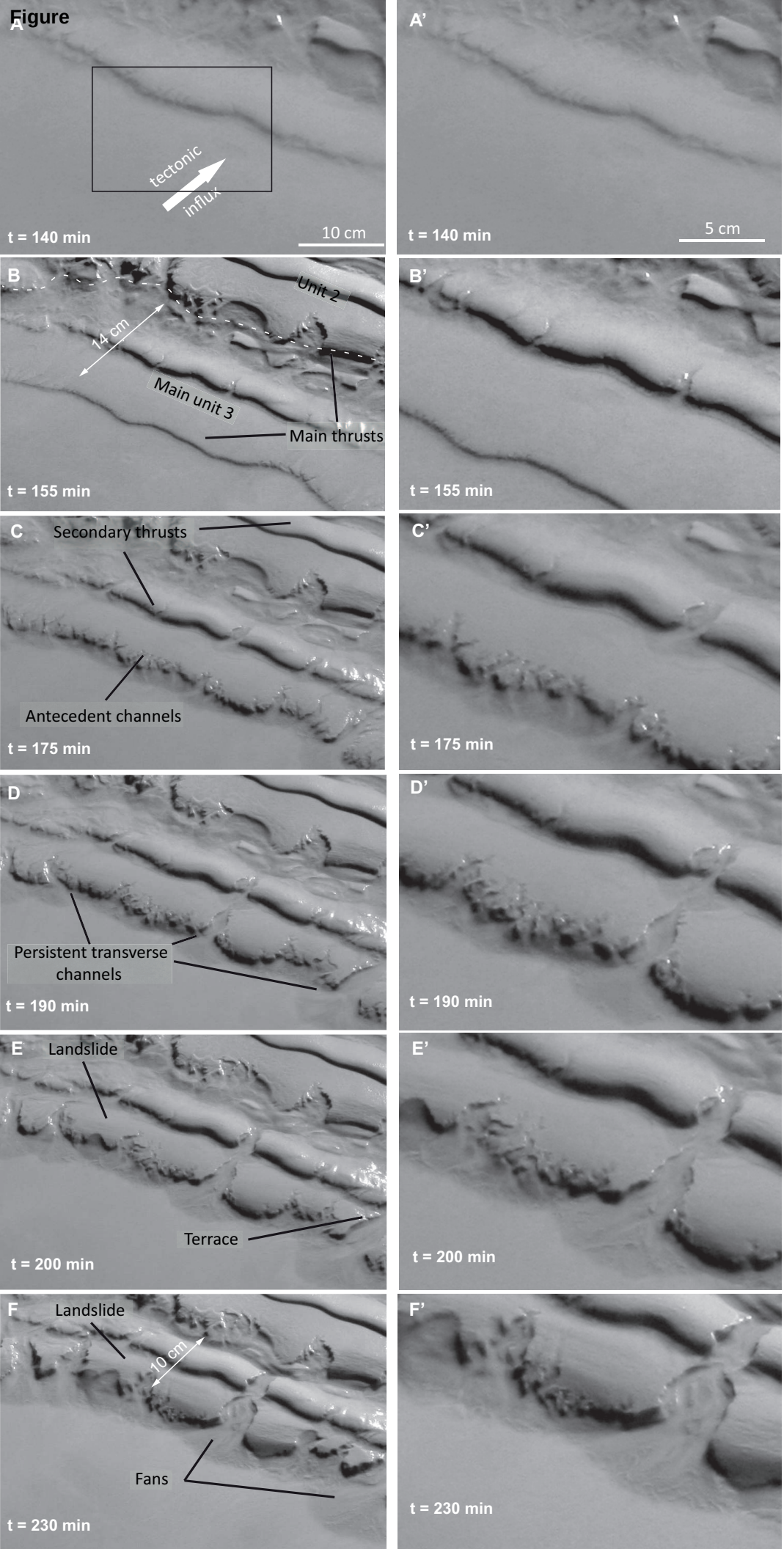
A
tectonic
influx
10 cm
t = 140 min
A'
5 cm
t = 140 min
B
Unit 2
14 cm
Main unit 3
Main thrusts
t = 155 min
B'
t = 155 min
C
Secondary thrusts
Antecedent channels
t = 175 min
C'
t = 175 min
D
Persistent transverse channels
t = 190 min
D'
t = 190 min
E
Landslide
Terrace
t = 200 min
E'
t = 200 min
F
Landslide
10 cm
Fans
t = 230 min
F'
t = 230 min

Figure

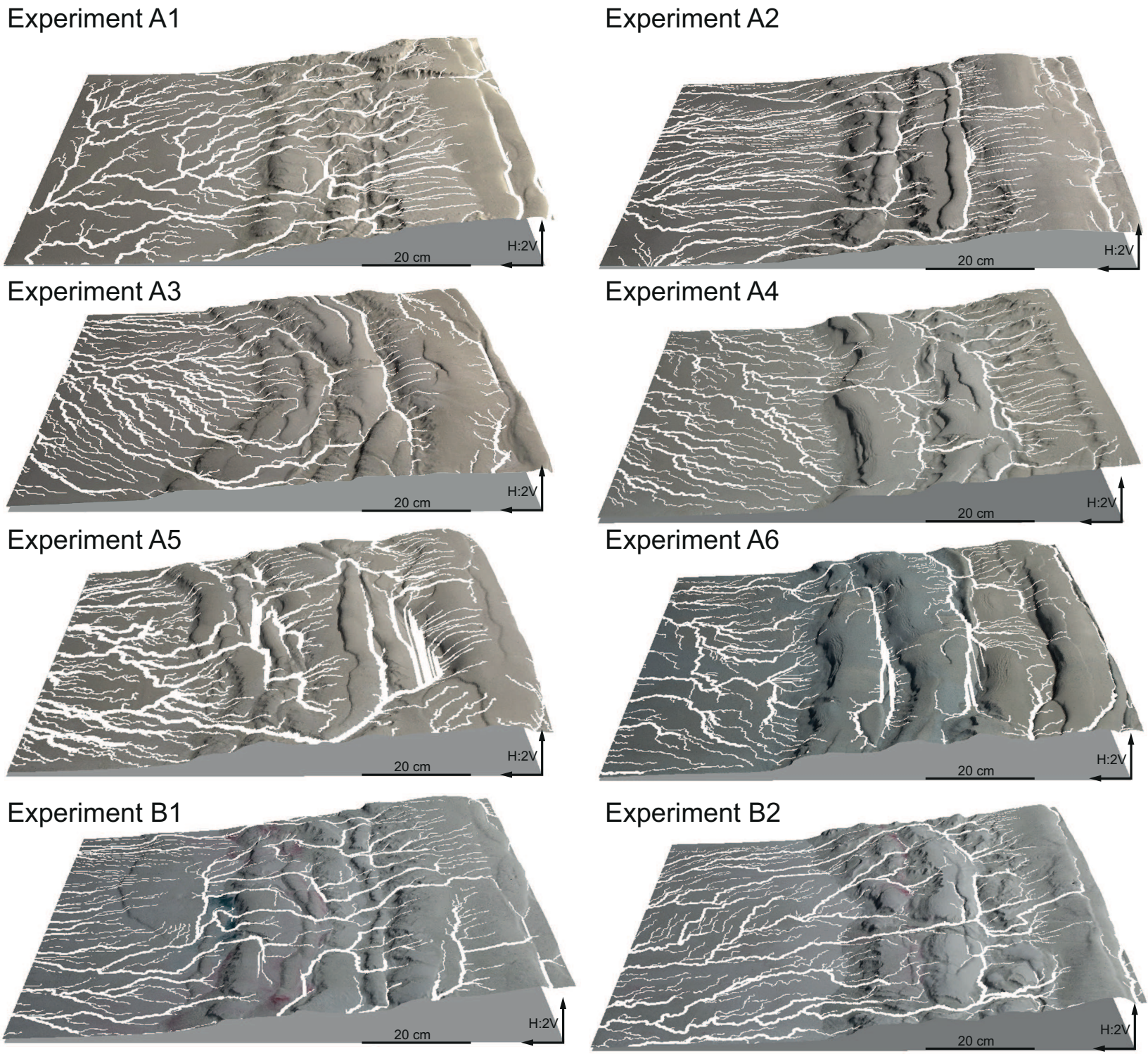
Experiment A1
20 cm
H:2V
Experiment A2
20 cm
H:2V
Experiment A3
20 cm
H:2V
Experiment A4
20 cm
H:2V
Experiment A5
20 cm
H:2V
Experiment A6
20 cm
H:2V
Experiment B1
20 cm
H:2V
Experiment B2
20 cm
H:2V

Figure

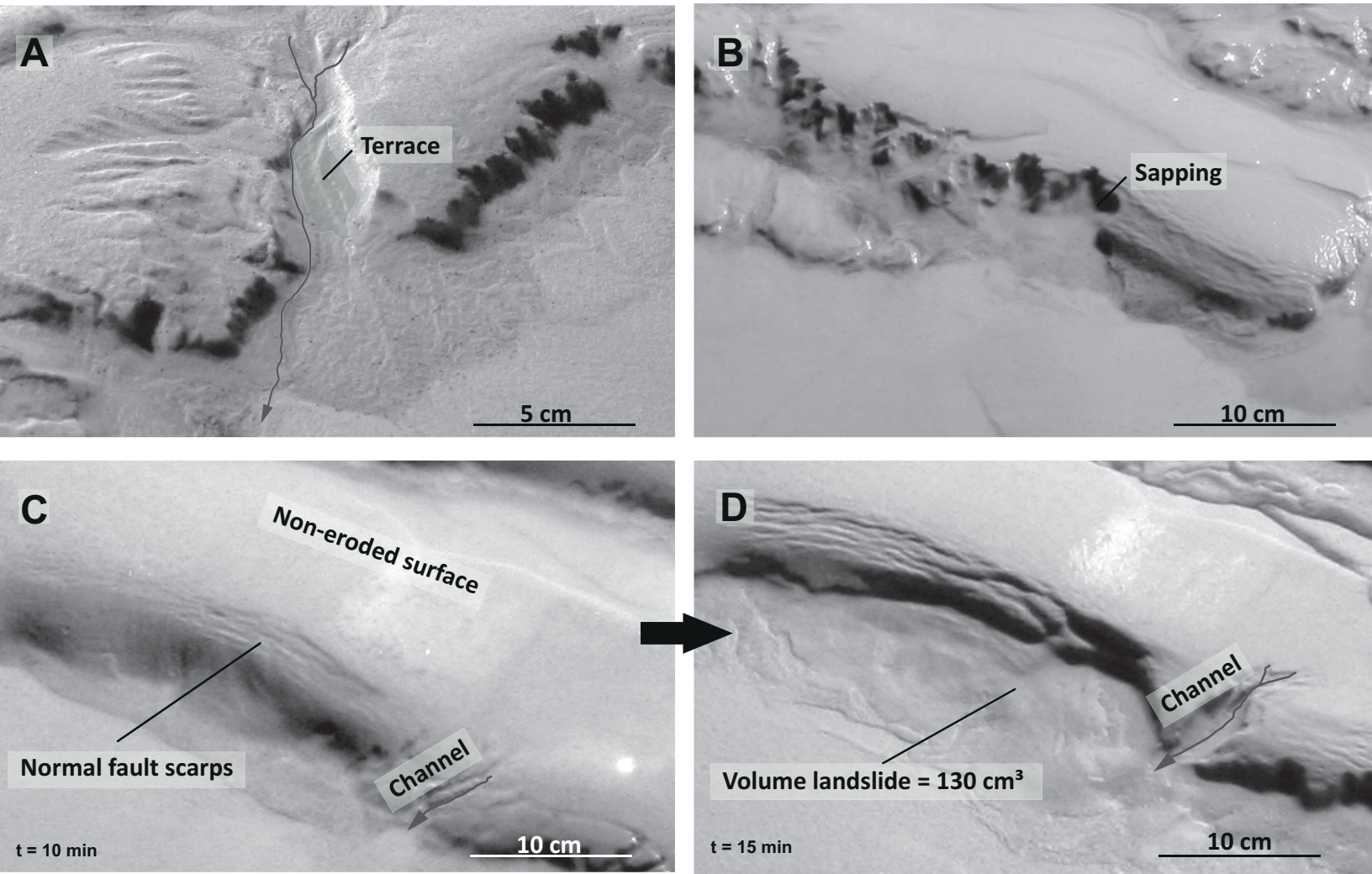
A
Terrace
5 cm
B
Sapping
10 cm
C
Non-eroded surface
Normal fault scarps
Channel
t = 10 min
10 cm
D
Channel
Volume landslide = 130 cm³
t = 15 min
10 cm

Figure

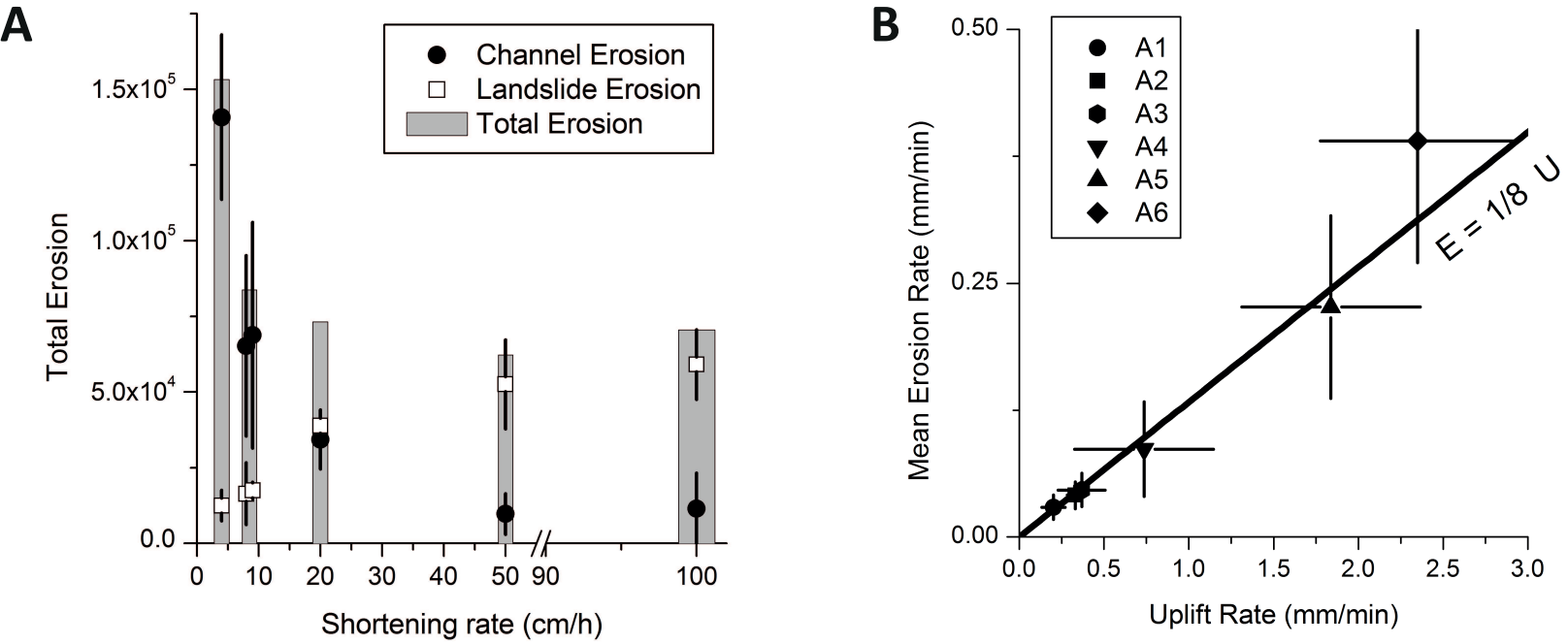
A
Channel Erosion
Landslide Erosion
Total Erosion
1.5x10^5
1.0x10^5
5.0x10^4
0.0
Total Erosion
0
10
20
30
40
50
90
100
Shortening rate (cm/h)
B
A1
A2
A3
A4
A5
A6
E = 1/8 U
0.50
0.25
0.00
Mean Erosion Rate (mm/min)
0.0
0.5
1.0
1.5
2.0
2.5
3.0
Uplift Rate (mm/min)

Figure
Click here to download high resolution image

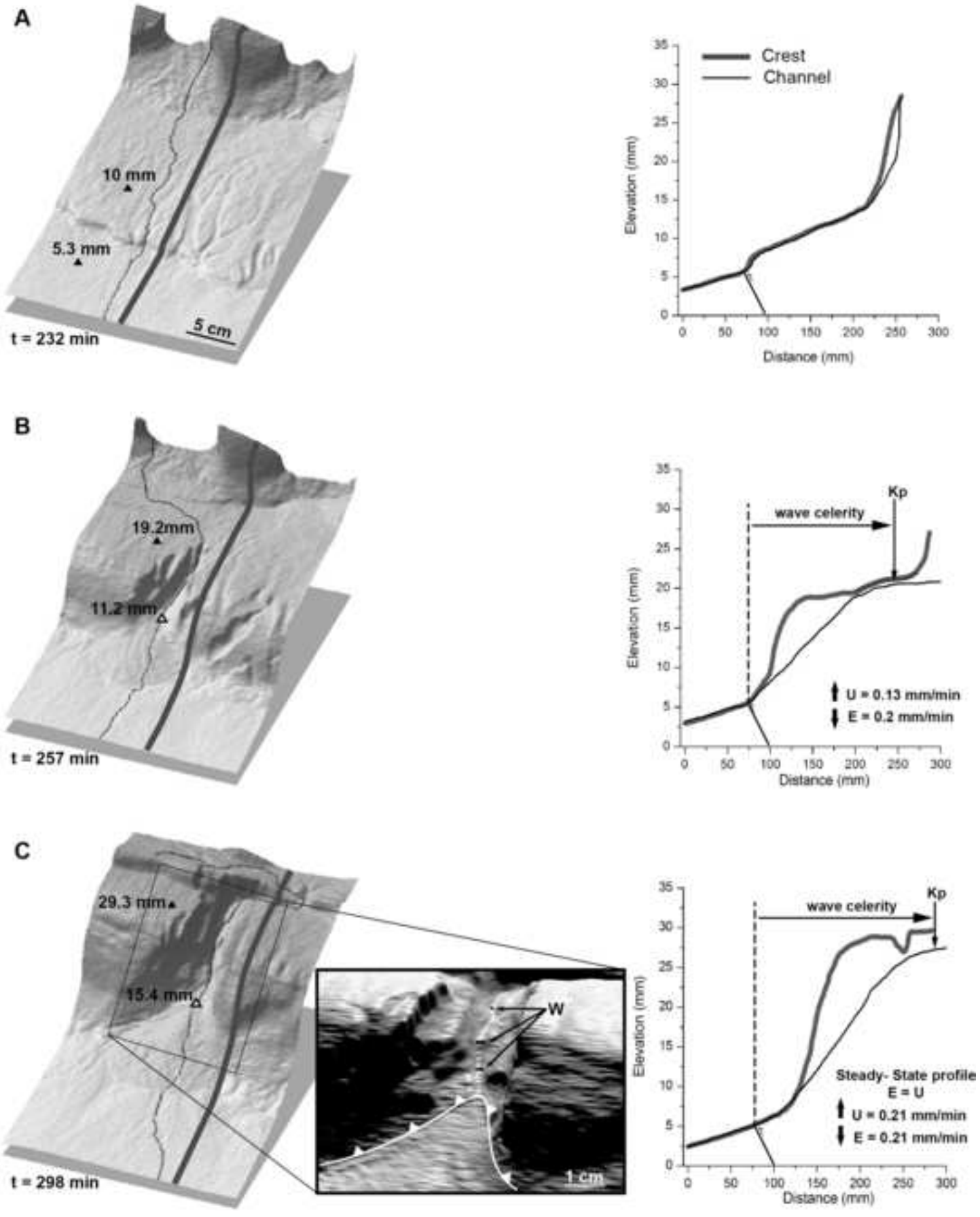

Figure

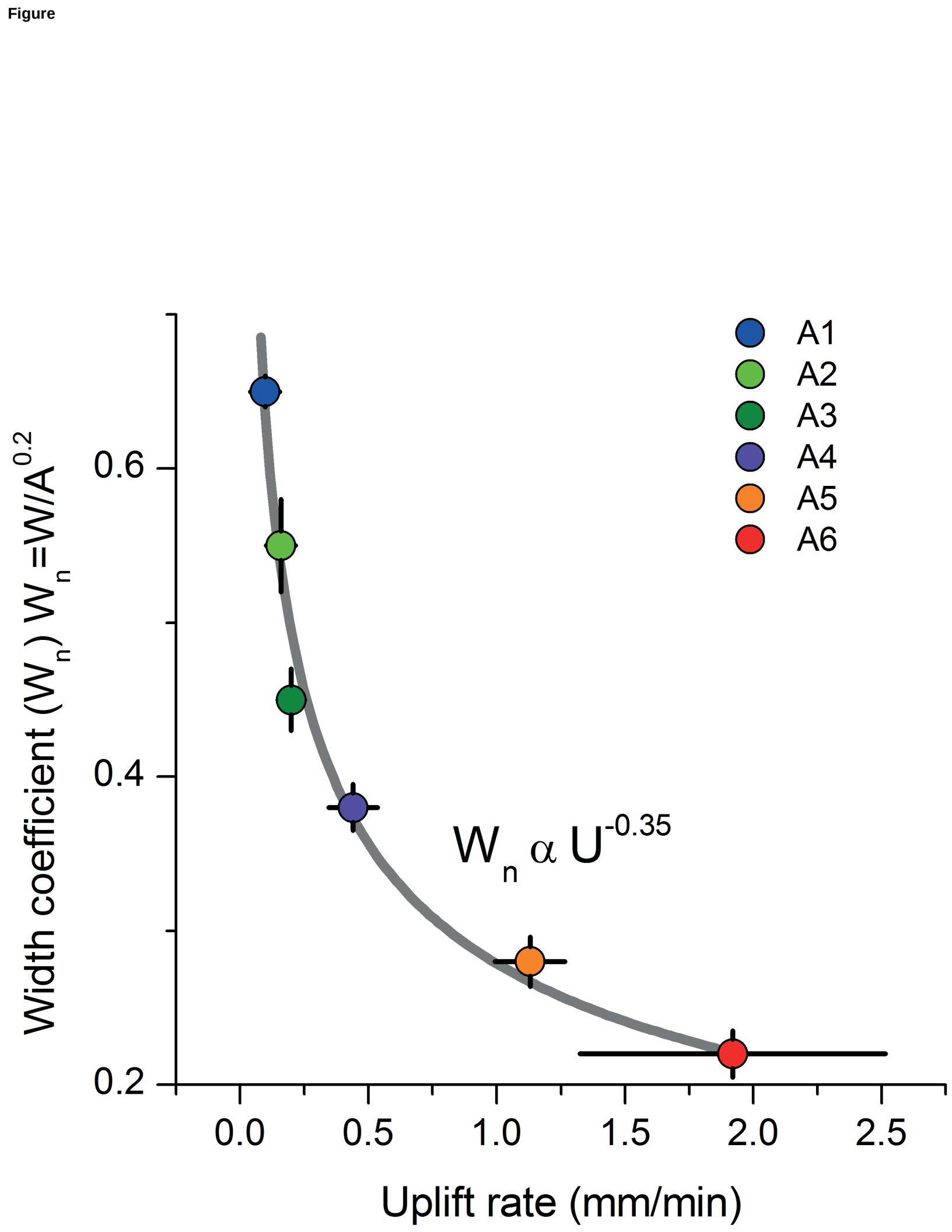
A1
A2
A3
A4
A5
A6
$W_n \alpha U^{-0.35}$
Width coefficient (W_n) $W_n = W/A^{0.2}$
0.2
0.4
0.6
0.0
0.5
1.0
1.5
2.0
2.5
Uplift rate (mm/min)

Figure

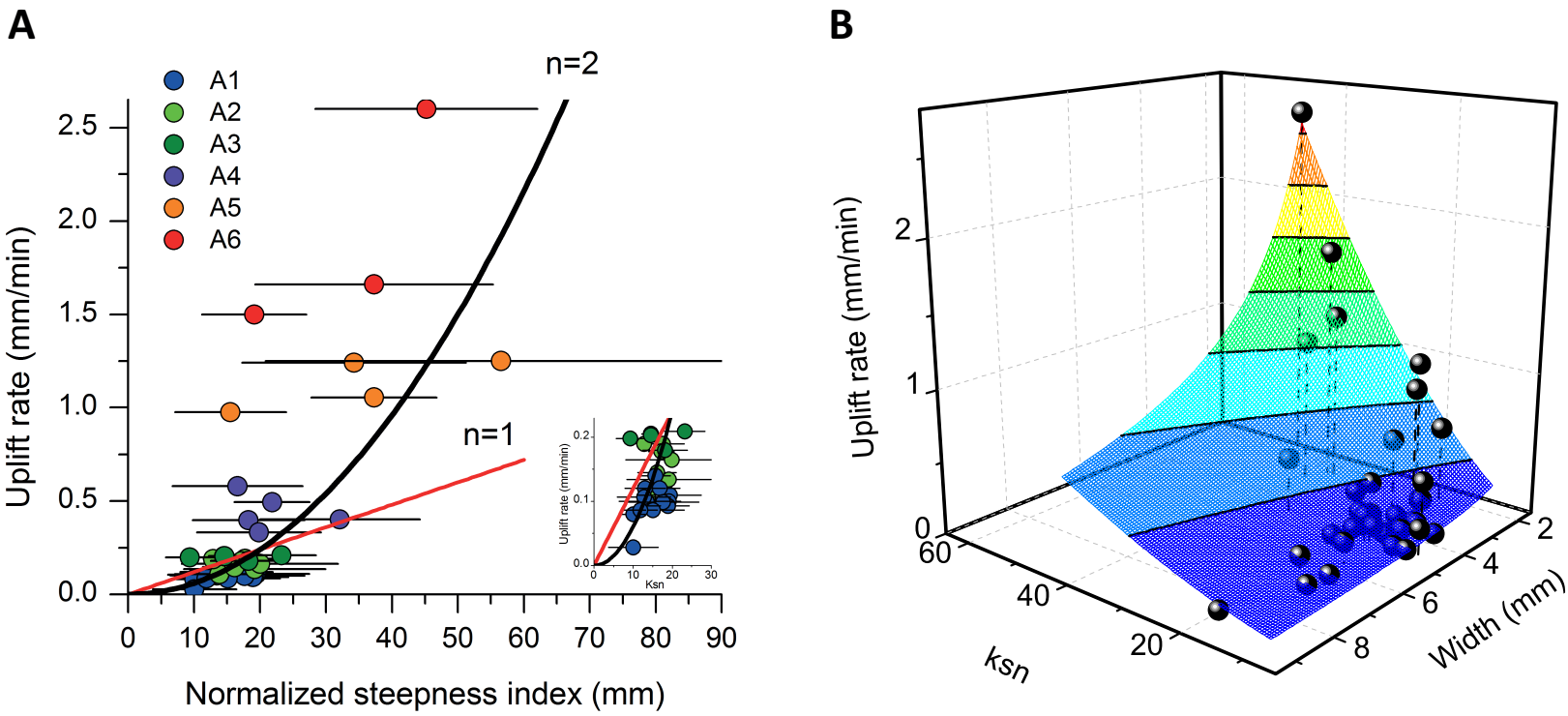
A
B
A1
A2
A3
A4
A5
A6
n=2
n=1
Uplift rate (mm/min)
Normalized steepness index (mm)
Ksn
ksn
Width (mm)

Figure

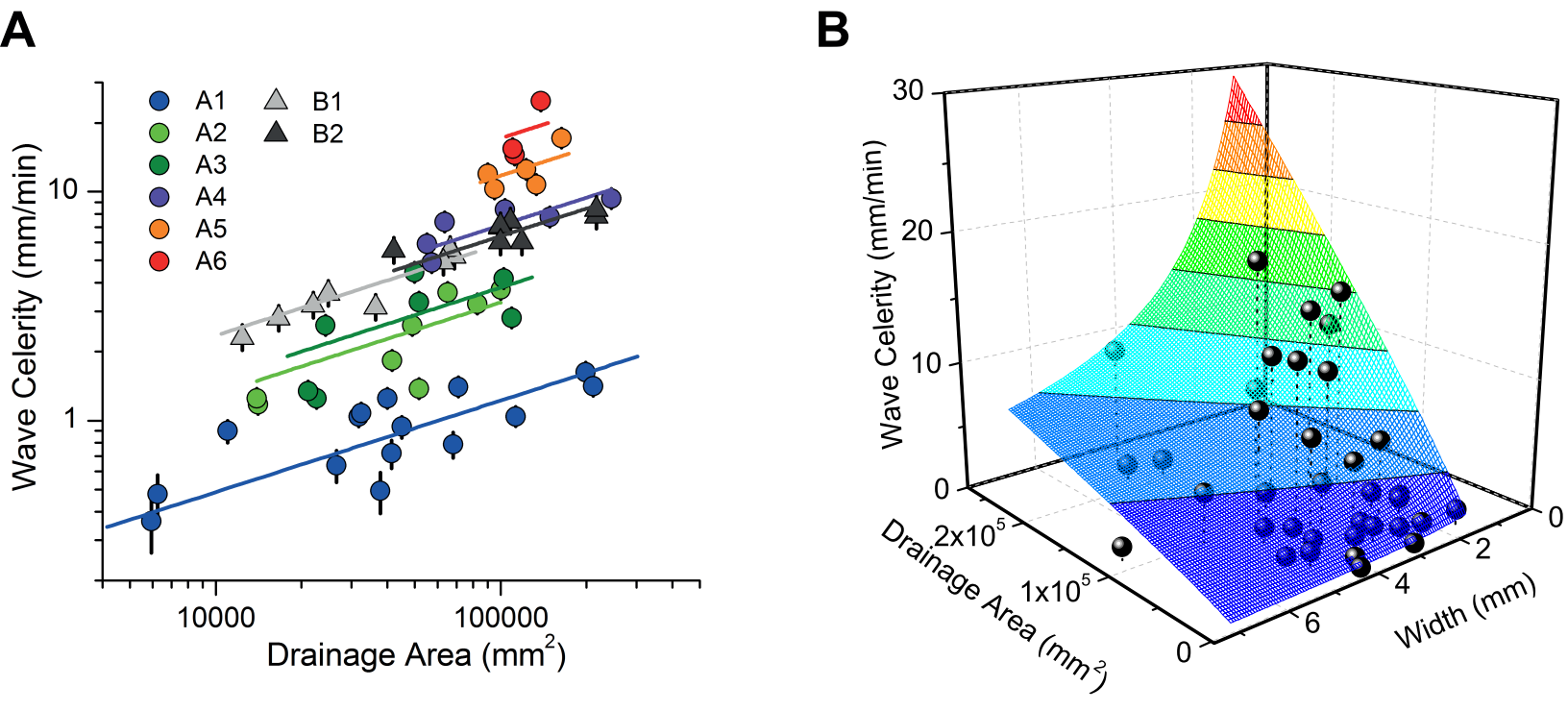
A
A1
A2
A3
A4
A5
A6
B1
B2
Wave Celerity (mm/min)
10
1
10000
100000
Drainage Area (mm²)
B
30
20
10
0
Wave Celerity (mm/min)
2x10⁵
1x10⁵
0
Drainage Area (mm²)
0
2
4
6
Width (mm)

Figure

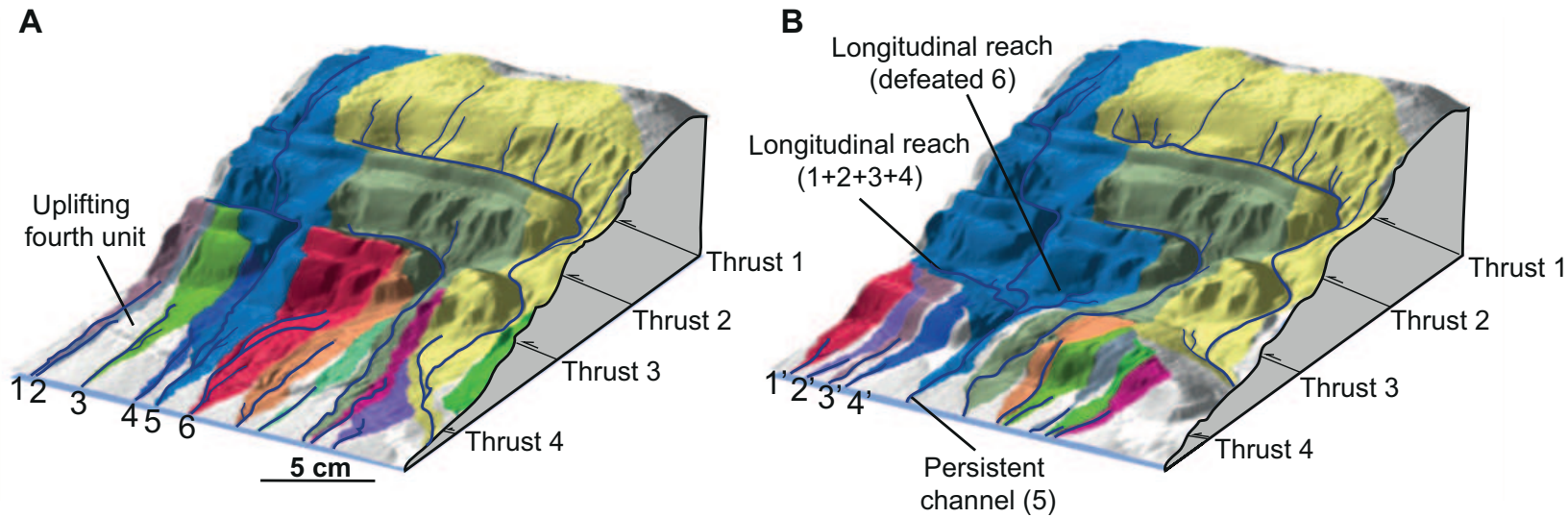
A
Uplifting
fourth unit
1 2 3 4 5 6
5 cm
Thrust 1
Thrust 2
Thrust 3
Thrust 4
B
Longitudinal reach
(defeated 6)
Longitudinal reach
(1+2+3+4)
1' 2' 3' 4'
Persistent
channel (5)
Thrust 1
Thrust 2
Thrust 3
Thrust 4

Figure

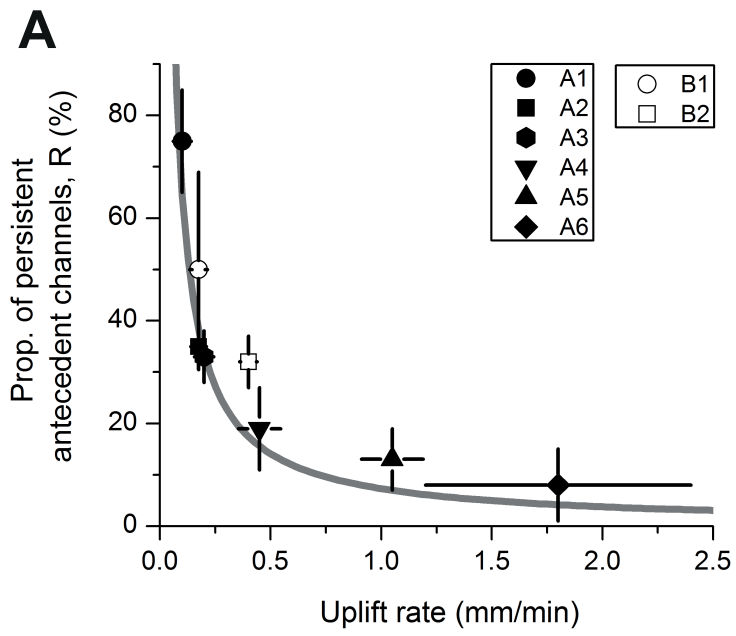
A
Prop. of persistent antecedent channels, R (%)
0
20
40
60
80
0.0
0.5
1.0
1.5
2.0
2.5
Uplift rate (mm/min)
A1
A2
A3
A4
A5
A6
B1
B2

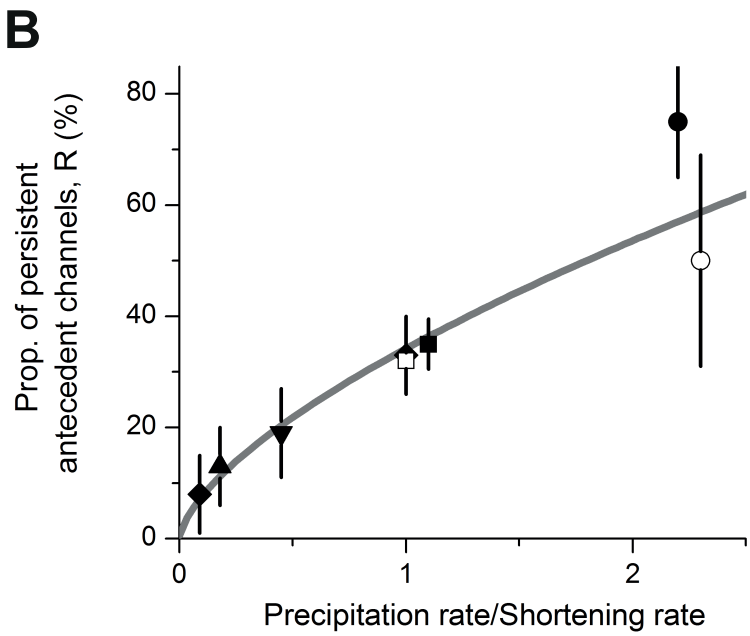
B
Prop. of persistent antecedent channels, R (%)
0
20
40
60
80
0
1
2
Precipitation rate/Shortening rate

Figure

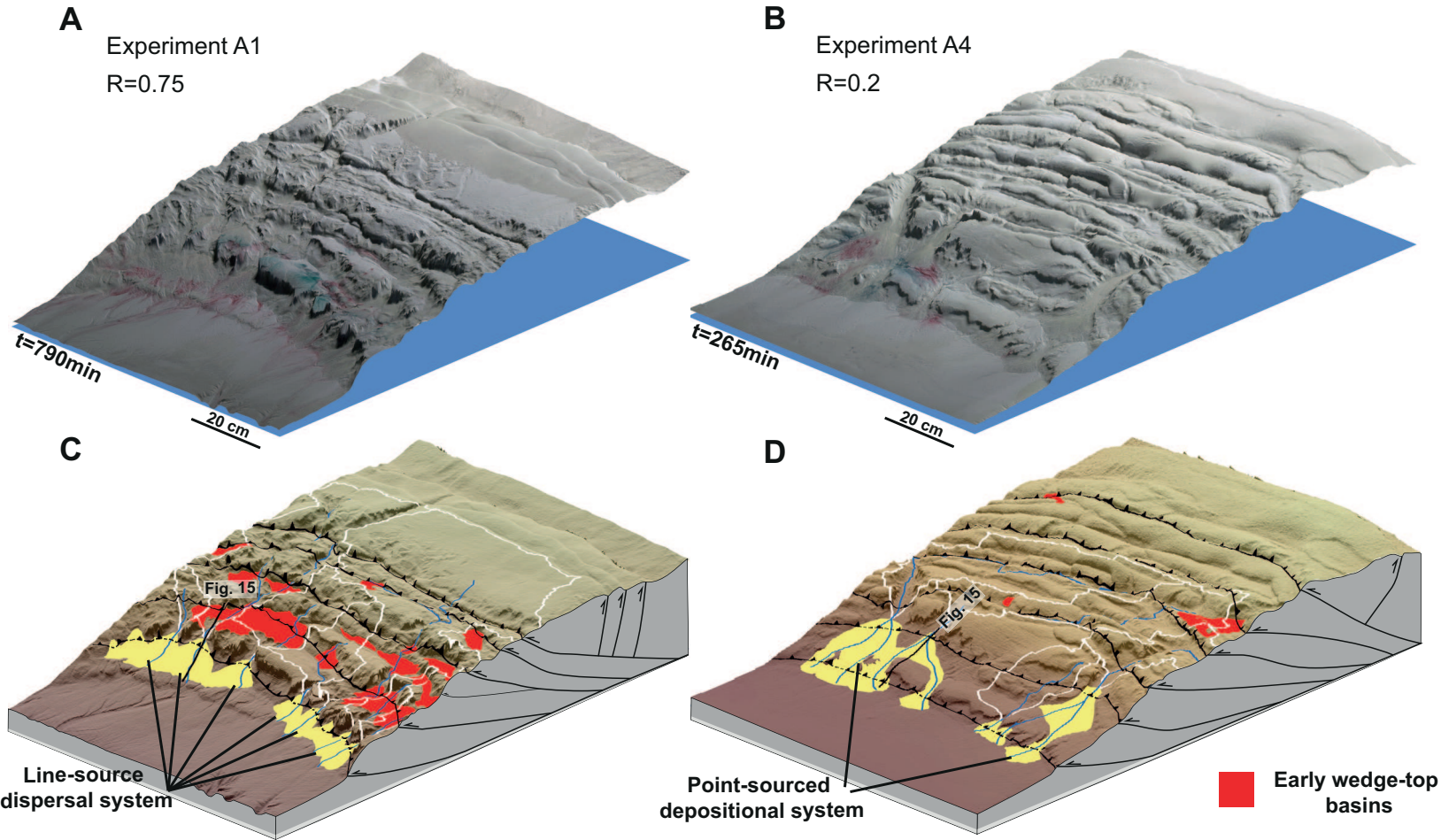
A
Experiment A1
R=0.75
t=790min
20 cm
B
Experiment A4
R=0.2
t=265min
20 cm
C
Fig. 15
Line-source
dispersal system
D
Fig. 15
Point-sourced
depositional system
Early wedge-top
basins

Figure

Click here to download high resolution image

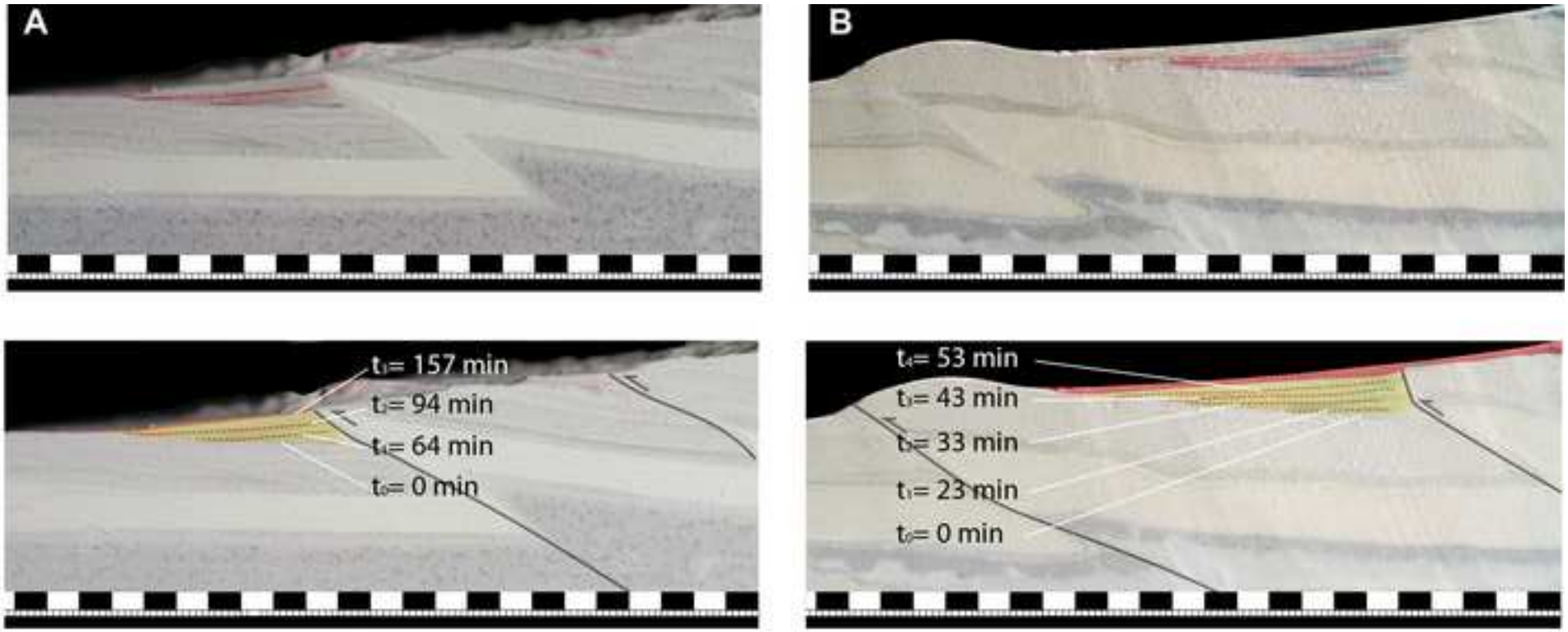

Figure

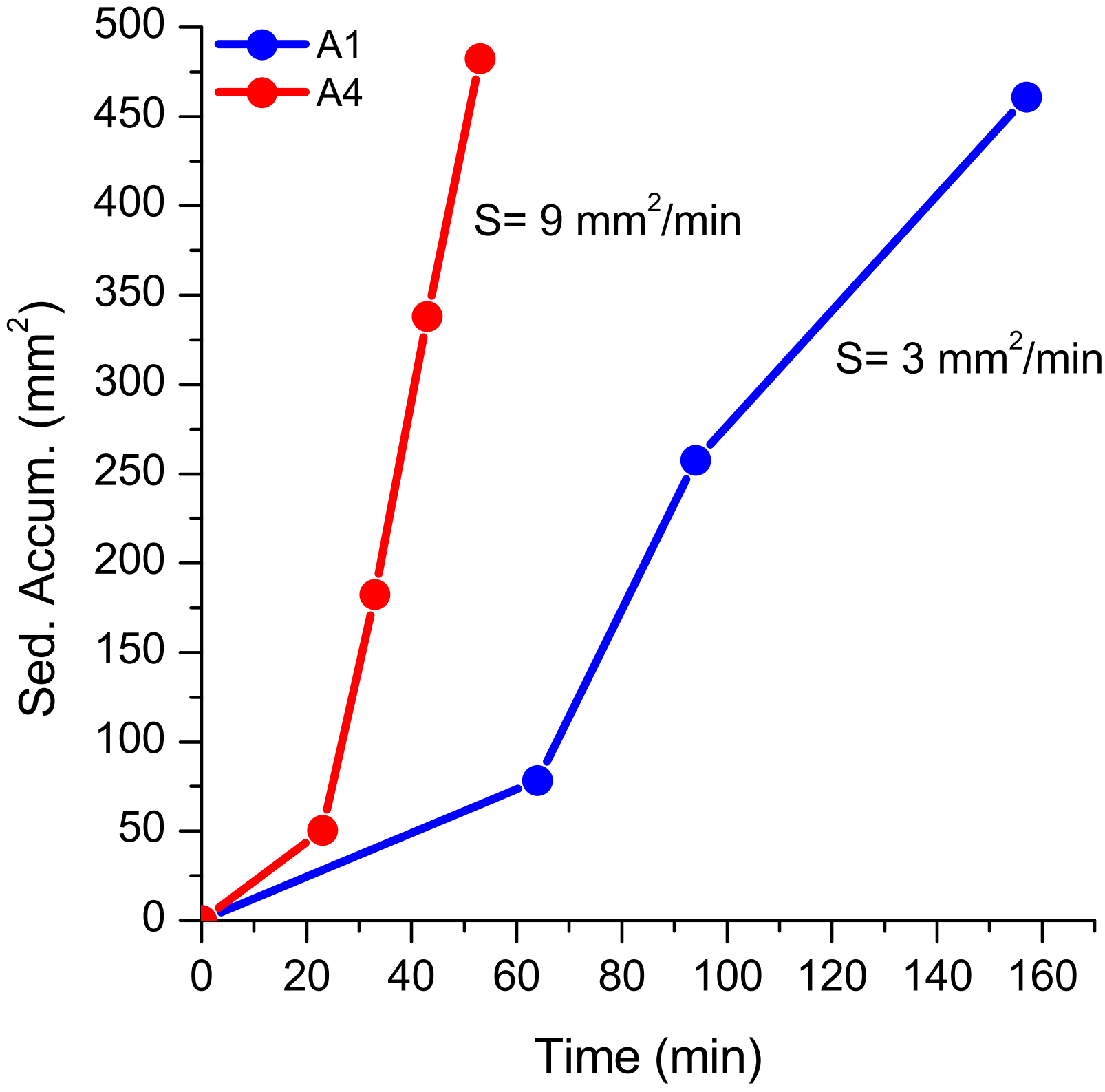
A1
A4
S= 9 mm²/min
S= 3 mm²/min
Sed. Accum. (mm²)
Time (min)
0
50
100
150
200
250
300
350
400
450
500
0
20
40
60
80
100
120
140
160

Figure

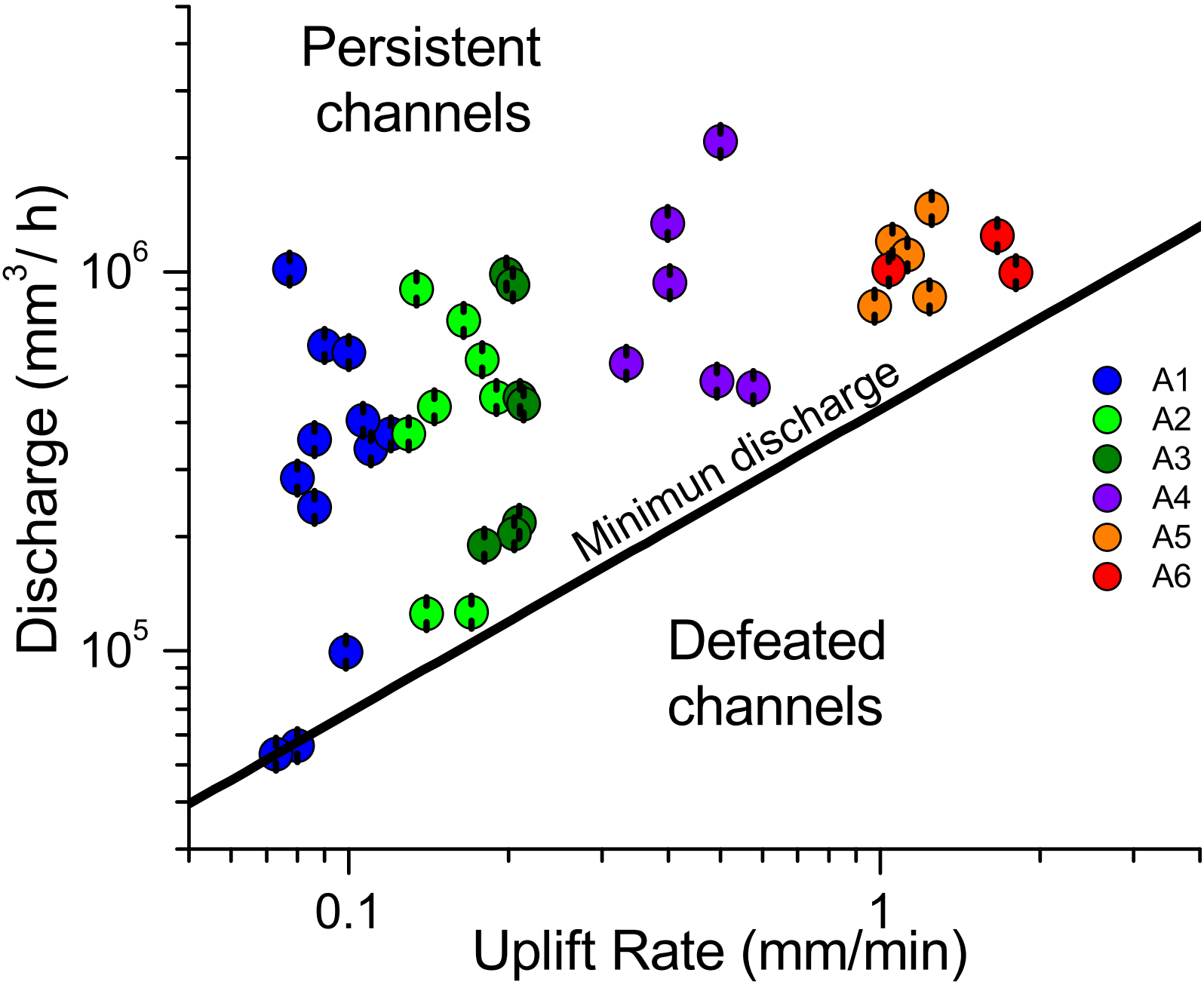
Persistent
channels
Minimun discharge
Defeated
channels
A1
A2
A3
A4
A5
A6
Discharge (mm3/ h)
10^6
10^5
0.1
1
Uplift Rate (mm/min)

Supplementary material for online publication only

Click here to download Supplementary material for online publication only: Animation1.mov

Supplementary material for online publication only

Click here to download Supplementary material for online publication only: Supplementary_Table.xlsx